

This is an Accepted Manuscript for *Journal of Glaciology*. Subject to change during the editing and production process.

DOI: 10.1017/jog.2024.38

# Transient subglacial water routing efficiency modulates ice velocities prior to surge termination on Sít' Kusá, AK.

Yoram TERLETH,<sup>1</sup> Timothy C. BARTHOLOMAUS,<sup>1</sup> Jukes LIU,<sup>2</sup> Flavien BEAUD,<sup>1</sup> T. Dylan MIKESELL,<sup>3</sup> Ellyn M. ENDERLIN,<sup>2</sup>

<sup>1</sup> *Department of Earth and Spatial Sciences, University of Idaho, USA*

<sup>2</sup> *Cryosphere Remote Sensing and Geophysics (CryoGARS) Laboratory, Department of Geosciences, Boise State University, USA.*

<sup>3</sup> *Norwegian Geotechnical Institute (NGI), Oslo, Norway.*

*Correspondence: Yoram Terleth <yterleth@uidaho.edu>*

## ABSTRACT.

Glacier surges are opportunities to study large amplitude changes in ice velocities and accompanying links to subglacial hydrology. Although the surge phase is generally explained as a disruption in the glacier's ability to drain water from the bed, the extent and duration of this disruption remain difficult to observe. Here we present a combination of in situ and remotely sensed observations of subglacial water discharge and evacuation during the latter half of an active surge and subsequent quiescent period. Our data reveal intermittently efficient subglacial drainage prior to surge termination, showing that glacier surges can persist in the presence of channel-like subglacial drainage and that successive changes in subglacial drainage efficiency can modulate active phase ice dynamics at timescales shorter than the surge cycle. Our observations favor an explanation of fast ice flow sustained through an out-of-equilibrium drainage system and a basal water surplus rather than binary switching between states in drainage efficiency.

This is an Open Access article, distributed under the terms of the Creative Commons Attribution-NonCommercial-NoDerivatives licence (<http://creativecommons.org/licenses/by-nc-nd/4.0/>), which permits non-commercial re-use, distribution, and reproduction in any medium, provided the original work is unaltered and is properly cited. The written permission of Cambridge University Press must be obtained for commercial re-use or in order to create a derivative work.

## 25 INTRODUCTION

26 Glacier surges are drastic, human-timescale changes in glacier behavior. They are characterised by semi-  
27 periodic, multi-year oscillations in ice velocities despite consistent, seasonal changes in melt input (e.g.  
28 Meier and Post, 1969; Truffer and others, 2021). Slow ice flow during quiescent phases ( $\sim 5$ - $>100$  years)  
29 alternates with 5- to 100-fold ice velocity increases during short active phases ( $\sim 1$ -30 years). Surge type  
30 glaciers cluster geographically within an envelope of climatic conditions (Sevestre and Benn, 2015). Surge  
31 type ice flow behavior is diverse but occurs on a continuous spectrum rather than within distinct categories,  
32 suggesting there is a unifying physical mechanism underlying glacier surging (e.g. Sevestre and Benn,  
33 2015). From a theoretical perspective, recent years have seen considerable progress towards uncovering  
34 such a universal model of glacier surging (Terleth and others, 2021). Approaches towards a universal  
35 model have included process-based considerations of evolving friction at the glacier bed (Thøgersen and  
36 others, 2019; Minchew and Meyer, 2020). Process-based models are promising avenues forward and more  
37 widely applicable models are emerging (Beaud and others, 2022). However, they do not yet explicitly  
38 include the important influence of changing water fluxes to and from the glacier bed during the surge  
39 cycle, although they do emphasize the importance of basal water pressure (Thøgersen and others, 2019;  
40 Minchew and Meyer, 2020; Beaud and others, 2022). A more systems based approach towards a unifying  
41 model of glacier surging is the enthalpy framework outlined in Benn and others (2019a). While the enthalpy  
42 framework incorporates both polythermal and temperate glaciers, it simulates ice flow acceleration through  
43 increased basal water pressure with a simplified sliding law. As such, the importance of hydraulic forcing  
44 to the surge mechanism is universally acknowledged in recent theories of glacier surging. Additionally,  
45 observational studies repeatedly note the influence of water presence and pressure at the glacier bed in  
46 driving surge dynamics (e.g. Kamb and others, 1985; Murray and others, 2000; Kotlyakov and others, 2004;  
47 Benn and others, 2019b).

48 Hydraulic forcing on ice velocities is not specific to glacier surging and largely depends on the bed's  
49 ability to evacuate water influxes from surface runoff (e.g. Iken and Bindenschadler, 1986), which in turn de-  
50 pends on the subglacial drainage system's configuration (e.g. Kamb, 1987). A variety of possible subglacial  
51 drainage systems exist within the literature, each with specific characteristics. While there is a spectrum  
52 of geometries and behaviors, most proposed drainage configurations fit loosely within one of two broad  
53 categories. The first grouping of drainage systems is distributed and inefficient, including flow through a



54 water film between the ice base and the substrate (Weertman, 1972), flow through porous substrates (e.g.  
55 Clarke, 1996; Flowers and Clarke, 2002; Kyrke-Smith and others, 2014), flow through poorly connected  
56 cavities (e.g. Lliboutry, 1968; Walder, 1986) or flow from the surface to unconnected cavities (e.g. Rada  
57 and Schoof, 2018; Nanni and others, 2021). Inefficient drainage systems tend to promote fast ice velocities  
58 due to their ability to sustain high basal water pressure. Increases in water pressure at the glacier base  
59 promote basal sliding through two mechanisms: changes in the ice-contact area with the bed surface by  
60 water-filled cavity growth (e.g. Iken, 1981; Anderson and others, 2004; Zoet and Iverson, 2015) and the  
61 dependence of subglacial till strength on effective pressure (e.g. Truffer and others, 2000; Tulaczyk and  
62 others, 2000; Iverson, 2010; Zoet and Iverson, 2020).

63 The second grouping of drainage systems includes configurations that transport water through localized  
64 and efficient channels forming at the glacier sole (Röthlisberger, 1972) or within the substrate (Nye, 1976).  
65 Channelized drainage systems adjust their morphology to changes in water influx from surface runoff and  
66 thus undergo only short lived (hours to days) increases in basal water pressure (e.g. Bartholomaus and  
67 others, 2008; Beaud and others, 2018). Efficient channelized systems tend to grow into dendritic patterns  
68 with limited spatial extent below glacier beds, as larger, lower pressure channels draw from smaller, higher  
69 pressure channels (e.g. Walder, 1986; Church and others, 2021; Nanni and others, 2021). Channel-like  
70 drainage systems are thought to evolve from distributed systems under sustained water supply (e.g. Hock  
71 and Hooke, 1993; Sundal and others, 2011). Once formed, they increase basal drainage efficiency and  
72 decrease basal water pressures, leading to a reduction in glacier velocities. This temporal evolution of  
73 basal drainage is a widely accepted mechanism for seasonal ice velocity changes, based on modelling studies  
74 (e.g. Schoof, 2010) and observational evidence (e.g. Tedstone and Arnold, 2012; Moon and others, 2014;  
75 Andrews and others, 2014). However, there are examples of channel-like systems in soft substrates that  
76 do not clearly transition to low pressure and high discharge regimes and that have the ability to restrict  
77 water flow over prolonged periods of time (Hock and Hooke, 1993; Walder and Fowler, 1994; Gulley and  
78 others, 2012; Hart and others, 2022).

79 The association between distributed, low efficiency drainage systems and high ice velocities hints at a  
80 mechanism explaining surging through persisting distributed and inefficient drainage. The most detailed  
81 description of such a hydrologically driven model of glacier surging was derived for the conditions of  
82 Variegated Glacier, Alaska (Kamb and others, 1985; Kamb, 1987). It suggests the active phase is sustained  
83 as long as there is a stable distributed drainage system of linked cavities that sustains high basal water

84 pressures and does not adapt its morphology to changes in water supply. The surge terminates with the  
85 destabilisation and collapse of these linked cavities in favor of a channelized drainage system, causing an  
86 abrupt release of the subglacial water volume (Kamb and others, 1985). The model's specificity to hard  
87 beds and the requirement of low water supply conditions prior to surge initiation somewhat limit its wider  
88 applicability (Harrison and Post, 2003). Explaining a wider range of surging behavior, such as surging  
89 under the presence of soft substrates (e.g. Hamilton and Dowdeswell, 1996; Truffer and others, 2000)  
90 or surge initiation during the melt season (Dunse and others, 2015; Sevestre and others, 2018), through  
91 changes in basal hydrology requires a reconsideration of the hydrologically driven surge model (Benn and  
92 others, 2022). In their observations of the 82–83 surge of Variegated Glacier, Kamb and others (1985)  
93 note large variations in borehole water level, in ice velocity, and in terminus stream discharge prior to  
94 surge termination (their Figs. 5, 9, and 10). This variability suggests a complexity in the evolution of the  
95 drainage system during a glacier's surge phase and a resilience of high basal pressure to temporary episodes  
96 of water release that is not yet fully captured in the Kamb (1987) single hydrological switch model. New,  
97 modern in situ observations of the evolution of the subglacial drainage system are a critical avenue towards  
98 a truly universal and more detailed reconsideration of the hydrologically driven surge model (e.g. Truffer  
99 and others, 2021).

100 Here, we present observations of a well-instrumented surge on a temperate glacier in Alaska. We  
101 combine time-series of seismic observations, ice velocities, and fjord water turbidity towards a partial  
102 record of subglacial drainage efficiency. Following a description of our data collection and the observational  
103 and model results, we devote the first part of our discussion to careful interpretation of each of the collected  
104 time-series signals (e.g., what time-series of seismic observations or of remotely sensed fjord color reveal  
105 about glacier behavior). In the second discussion section, following the attribution of observations to  
106 processes, we consider these processes in relation to one another and discuss the role of successive changes  
107 subglacial drainage in modulating surge dynamics. We place the significance of our findings in the context  
108 of previous work, and suggest potential implications for the surge mechanism. The complex variability in  
109 drainage efficiency prior to surge termination hints that conceptual models of drainage system evolution  
110 during the surge cycle may need expanding.

## 111 **STUDY SITE**

112 Our work centers around the 2020-2021 surge of Sít' Kusá (briefly known as Turner Glacier), located on  
113 Tlingit land in the St. Elias range in Wrangell-St. Elias National Park, Alaska (Fig.1). The ~30 km  
114 long and ~2 km wide Sít' Kusá, which translates from Tlingit to "Narrow Glacier", consists of multiple  
115 tributaries, with two main branches merging into a main trunk. This main trunk flows to sea level and  
116 terminates on a sediment shoal between surges and at tidewater in Disenchantment Bay during surge-  
117 driven advances. Surges initiate in the northernmost main tributary and propagate downglacier towards  
118 the terminus. Sít' Kusá exhibits active phases of 1 to 2 years and quiescent phases of ~6 years, making it  
119 the most frequently surging glacier described in the literature (Nolan and others, 2021). The most recent  
120 surge initiated in March 2020, with velocities increasing from ~3 m d<sup>-1</sup> to ~25 m d<sup>-1</sup> in the lower northern  
121 tributary (Liu and others, 2024). An extensive array of instrumentation was installed on and around the  
122 glacier in late August of 2020 (Fig.1). The surge front reached the glacier terminus in October 2020 (Liu  
123 and others, 2024), and the surge remained active until termination during the 2021 melt season, when  
124 surface velocities decreased to <5 m d<sup>-1</sup> and generally remained at ~1 m d<sup>-1</sup>.

## 125 **DATA ACQUISITION AND ANALYSIS**

### 126 **Glaciohydraulic Tremor**

127 We aim to identify change in the subglacial hydrological system by monitoring seismic tremor, i.e. low am-  
128 plitude seismic signals with consistent spectral content and durations of hours to months, around the glacier  
129 (Bartholomaus and others, 2015). In light of topographical constraints, twelve broadband seismometers  
130 were deployed as evenly spaced as possible at locations surrounding the main trunk of the glacier (Fig.1).  
131 Sensors are named according to their placement on the East or West side of the glacier, and their distance  
132 in kilometers from the glacier terminus. All sensors were buried at depths of ~40 cm in glacier-proximal  
133 sediment. Eight stations provide high-quality, continuous records over nearly 24 months, while four stations  
134 suffered either wildlife damage (similar to that described in Tape and others, 2019) or other instrument  
135 malfunction (Fig.1b).

136 Seismic stations included Nanometrics Trillium Compact Posthole and Nanometrics Meridian Compact  
137 Posthole seismometers, sampling at 250 Hz and with 20-s and 120-s low frequency corners, respectively.  
138 Throughout this study, we analyze instrument-corrected vertical-component data. Prior to deployment, all

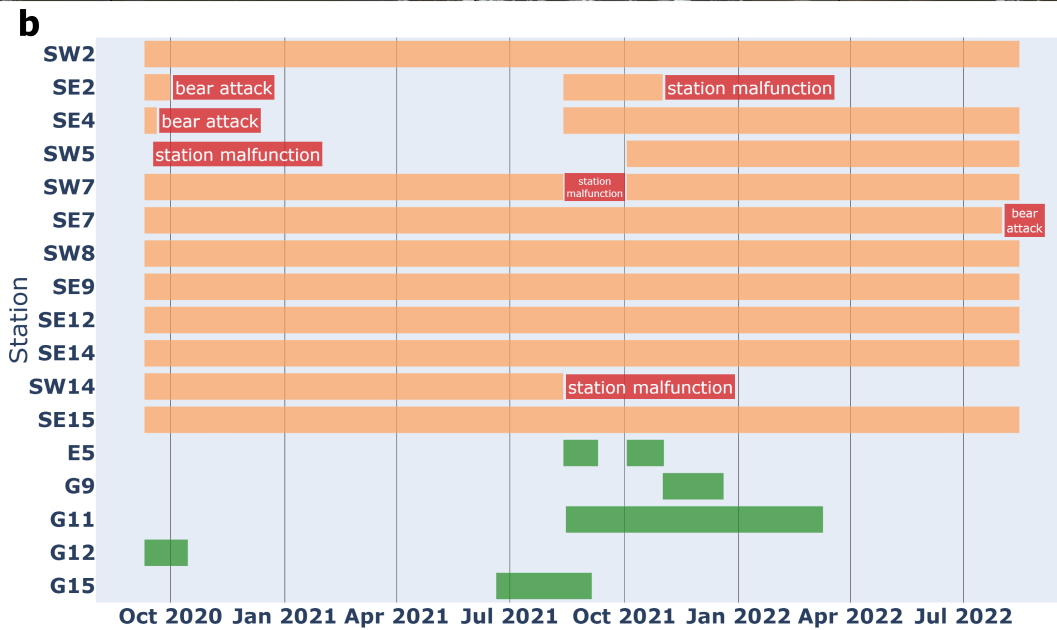
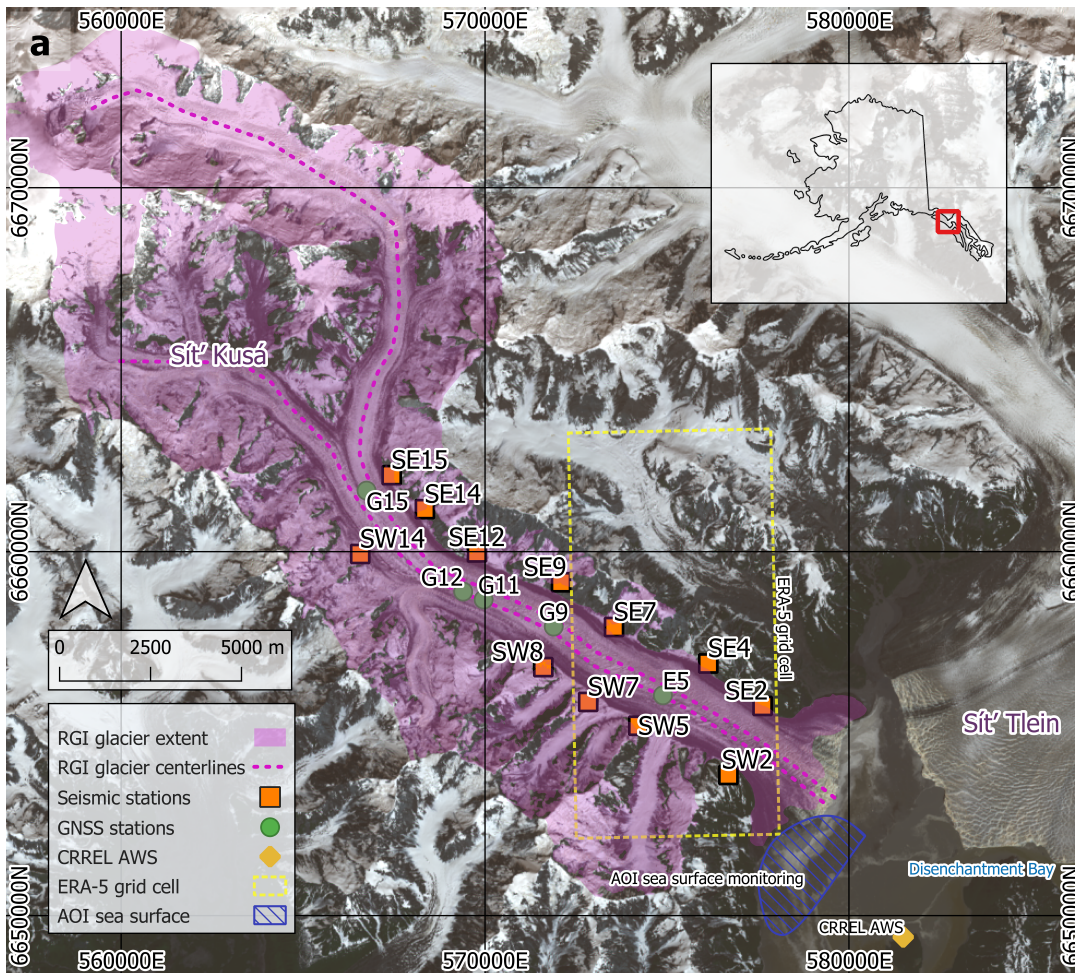


**Fig. 1.** a) Main components of deployed instrument network. Glacier extent and centerlines from RGI database. Background imagery is a Landsat-8 OLI scene acquired on 18 July 2021. Inset shows location in Alaska. Grid is in the coordinate reference system (CRS): UTM 7N, EPSG:32606. The datum is WGS 84. b) Gantt chart showing temporal coverage of deployed network.



139 sensors were tested for uniformity and show inter-comparable seismic power (within  $\pm 0.2$  dB) at frequencies  
140 above 0.1 Hz. Here we draw on data from three stations with continuous records that span the instrumented  
141 reach of the glacier. The record of these three stations is representative of the rest of our deployed network  
142 (Fig.S1.1, Fig.S1.2), and our findings are reproducible with other stations.

143 We follow the methodology outlined in Bartholomaus and others (2015) and shared via Bartholomaus  
144 and Terleth (2023) to quantify the strength of seismic tremor that has previously been associated with  
145 glaciohydraulic sources. For each station, we compute the power spectral density (PSD) of 20 second  
146 windows with 50% overlap. We then compute the median power over one hour long time-windows with  
147 50% overlap. This yields a median valued PSD every 30 minutes (i.e. 48 PSDs in 24 hours), as illustrated  
148 in the example spectrograms in Fig.2a) and b. In Bartholomaus and others (2015), power within the 1.5-10  
149 Hz frequency range is attributed to glaciohydraulic tremor. However, the 0.5-3 Hz frequency range is also  
150 influenced by calving events (O'Neel and Pfeffer, 2007; Bartholomaus and others, 2012). The high number  
151 of calving events in Disenchantment Bay noticeably impact the median spectra below 3 Hz (Fig.2 c and d,  
152 Text S2, Fig.S2.1), so we focus on the frequency band of 3-10 Hz to isolate glaciohydraulic tremor and sum  
153 and standardize the PSD power within this band to obtain the glaciohydraulic tremor time-series shown  
154 in Fig.2c and in Fig.S1.2. Similar considerations of frequency ranges  $>3$  Hz have been used successfully to  
155 monitor glaciohydraulic tremor in Nanni and others (2020) and Lindner and others (2020).

## 156 **Lags in the Downglacier Tremor Signals**

157 Beyond temporal changes, we are interested in observing spatial variability in recorded tremor. The spatial  
158 extent and density of the deployed seismic array is too wide to effectively conduct precise location tracking  
159 of tremor sources over time, (e.g. Nanni and others, 2021; Labeledz and others, 2022), but it does allow for  
160 inter-station comparisons of the PSDs in terms of temporal lag between glaciohydraulic tremor signals. We  
161 favor this approach over dominant noise source tracking (Vore and others, 2019) because for our purposes  
162 we are interested in the spatial propagation of tremor signals rather than the location of the highest  
163 amplitude tremor source. We use wavelet coherence analysis (Grinsted and others, 2004) to determine  
164 similarity between the time-series of station power spectral densities in time frequency space. We assume  
165 that the median spectral power between 3 and 10 Hz received at any given station is dominated by source(s)  
166 proximal to the station. This assumption is more valid for stations that are spatially distant: glaciohydraulic  
167 tremor signals have not been detectable at ranges  $>1-3$  km in previous studies (Bartholomaus and others,

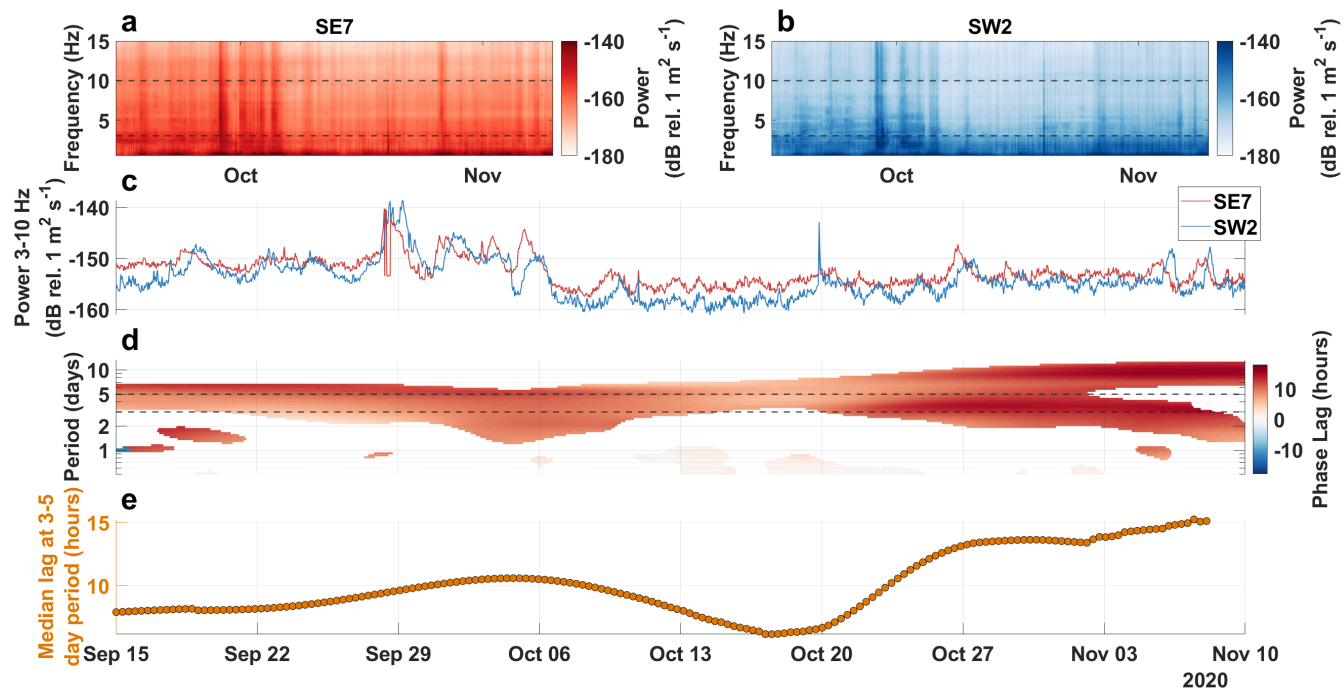


**Fig. 2.** Illustration of the analysis process that yields time-lags and velocities of a seismic tremor pulse. a) Median spectrogram for SE7. b) Median spectrogram for SW2. Dotted lines show frequency bounds between which we consider glaciohydraulic tremor. c) Time-series of PSD amplitudes for SE7 and SW2 summed between 3-10 Hz in each one hour time-window, with 30-minutes overlap. d) Wavelet-based lag time estimation between signals recorded at SE7 and SW2, through time for different periods of oscillation. Positive (red) lags mean SE7 signal occurs before SW2 signal. Lags are plotted if coherence  $>0.7$ . Dashed lines show oscillation period corresponding to synoptic variability, 3-5 days. e) Time-series of median lag between SE7 and SW2 for coherent signals with periods between 3-5 days.

168 2015; Vore and others, 2019), meaning signals recorded at stations  $> 2-6$  km apart are likely independent.

169 Wavelet coherence analysis produces two outputs in time and frequency space: (1) coherence values between

170 zero and one, which reflect the similarity between the two signals, and (2) time-lag values which reflect

171 the time-shift needed to obtain the highest similarity between the two signals (Fig.2d). The time-lags are

172 masked when the coherence between the signals at a given periodicity is below 0.7, to ensure the obtained

173 lags are based on signals with a high degree of similarity. We focus on oscillations with a 3-5 day period as

174 this captures the main variability within the glacio-hydraulic tremor signals (Fig.2c). In order to obtain a

175 time-series of time-lags, we integrate the time-lags over the oscillation period by taking the median value

176 of the lags between the 3 and 5 day period bounds, drawn in dotted lines on Fig.2d. This yields a single

177 lag time value for each period over which there are high coherence lags (Fig.2e).

## 178 Surface Runoff

179 To estimate variation in surface meltwater supply to the subglacial environment, we apply the Energy  
180 Balance Firn Model (van Pelt and Oerlemans, 2012) to Sít' Kusá. The model solves the surface energy  
181 balance to compute surface temperature and melt values. The energy balance model is dynamically coupled  
182 to a physically based multi-layer snow and firn model that accounts for snow and firn pack densities,  
183 temperatures, water content, and vertical liquid water transport (e.g. van Pelt and others, 2012, 2021).  
184 The model thus accounts for water retention in snow and firn, which can significantly impact the timing  
185 and volume of surface melt delivery to the englacial water system (Vallot and others, 2017; van Pelt and  
186 others, 2018; Alexander and others, 2020). Sít' Kusá is estimated to receive as much as 7.5 m of annual  
187 precipitation (Simpson and others, 2005), much of it as snow, thus the incorporation of water storage in  
188 snow is an important component of the energy balance firn model. We expect there to be little delay in  
189 englacial water transfer during the considered time period as the glacier was already heavily crevassed in  
190 August 2020 (cf. Dunse and others, 2015; Gong and others, 2018), making the modelled surface runoff a  
191 relatively good estimate of the variability in water supply to the subglacial drainage system.

192 We force the energy balance firn model with meteorological data acquired at an automatic weather  
193 station located on Haenke Island (Fig.1) that is maintained and operated by the Cold Regions Research  
194 and Engineering Laboratory (Finnegan, pers. comm.). Precipitation, cloud cover, and relative humidity  
195 are required as model input data but are not recorded at the automatic weather station. For these vari-  
196 ables we use data from the corresponding grid cell of the European Centre for Medium-Range Weather  
197 Forecasts reanalysis version 5 product (Fig.1; Table S3.1). The energy balance firn model is distributed  
198 onto ArcticDEM, a high resolution digital surface model of the Arctic (Porter and others, 2018), with  
199 a 32 m spatial resolution. We simulate the period between January 2017 and August 2022 and we as-  
200 sess model performance through its ability to reproduce surface elevation change derived from Worldview  
201 high-resolution satellite imagery acquired during the 2022 melt season (Text S3b, Fig.S3.1). We further  
202 include downglacier water routing by using the flow accumulation tool from the Matlab based topotool-  
203 box (Schwanghart and Scherler, 2014). We assume transfer of surface runoff to the glacier bed happens  
204 instantaneously through the severely crevassed glacier; we then use the subglacial hydropotential (Shreve,  
205 1972) as input for the flow accumulation computation in order to estimate total surface runoff upstream  
206 of any given point on the modelled grid (Text S3c). We assume uniform water pressure at the overburden  
207 pressure and use bed topography derived by subtracting ice thickness modelled in Millan and others (2022)



208 from ArcticDEM.

## 209 **Subglacial water discharge at the terminus**

210 Previous work has shown the feasibility of using remote sensing imagery to obtain a qualitative under-  
211 standing of frontal water release through time (Chu and others, 2009; McGrath and others, 2010; Tedstone  
212 and Arnold, 2012; Schild and others, 2017; Benn and others, 2019b). The Sít' Kusá terminus sits on a  
213 sediment shoal with water depths <40 m (Goff and others, 2012), the edge of which limits its advance into  
214 Disenchantment Bay during active phases. While we do not have a quantitative record of proglacial water  
215 discharge, we use sea surface characteristics of the area in front of the terminus of Sít' Kusá as a proxy  
216 for relative changes in subglacial discharge. During quiescent phases, a calving embayment consistently  
217 forms on the southern half of Sít' Kusá's calving front (Fig.3a). The formation of such embayments has  
218 been attributed to subglacial discharge release in previous work (Sikonia and Post, 1980; Fried and others,  
219 2018). At Sít' Kusá, the location of this embayment coincides with the most likely discharge channel based  
220 on hydropotential mapping (Fig.3a). Therefore, we manually delimit a  $\sim 6.5 \text{ km}^2$  area of sea surface in  
221 front of the calving embayment and use this region as our area of interest (AOI) to assess water discharge.  
222 We use the average pixel values within the AOI for band 7 of the Sentinel-3 Ocean and Land Color Imager  
223 (OLCI) Level-1b product as a proxy for sediment loading (ESA, 2022c). Band 7 records radiance within  
224 wavelengths of 615 to 625 nm (orange light in the visible spectrum), the spatial resolution of the pixels is  
225  $300 \times 300 \text{ m}$ , and at the latitude of Sít' Kusá there is a temporal resolution below one day. To increase the  
226 robustness of the derived time-series of sediment loading, we also investigate the surface reflectance pro-  
227 vided by the Sentinel-2 Multi-Spectral Instrument Level-2A band 4 centered at 665 nm (ESA, 2022b). The  
228 reflectance of water surfaces at these wavelengths scales closely with water turbidity (e.g. Schild and others,  
229 2017; Hossain and others, 2021) and should thus reflect relative changes in turbidity in our area of interest.  
230 All imagery is filtered for clouds using the provided data flags. The two time-series are well-correlated  
231 ( $r = 0.76$ ) between January 2019 and June 2022 (Fig.3).

232 To further assess the validity of our record as a proxy for sub-aqueous frontal discharge, we also create  
233 time-series of backscatter in vertical-vertical polarization from the Sentinel-1 C-band synthetic aperture  
234 radar (ESA (2022a); Fig.3e). The intensity of back-scatter from a water surface is expected to increase  
235 primarily with the presence of ice within the water (e.g. Ferdous and others, 2018; Benn and others, 2019b).  
236 As such, we expect the backscatter intensity to increase with calving during the melt season but to decrease

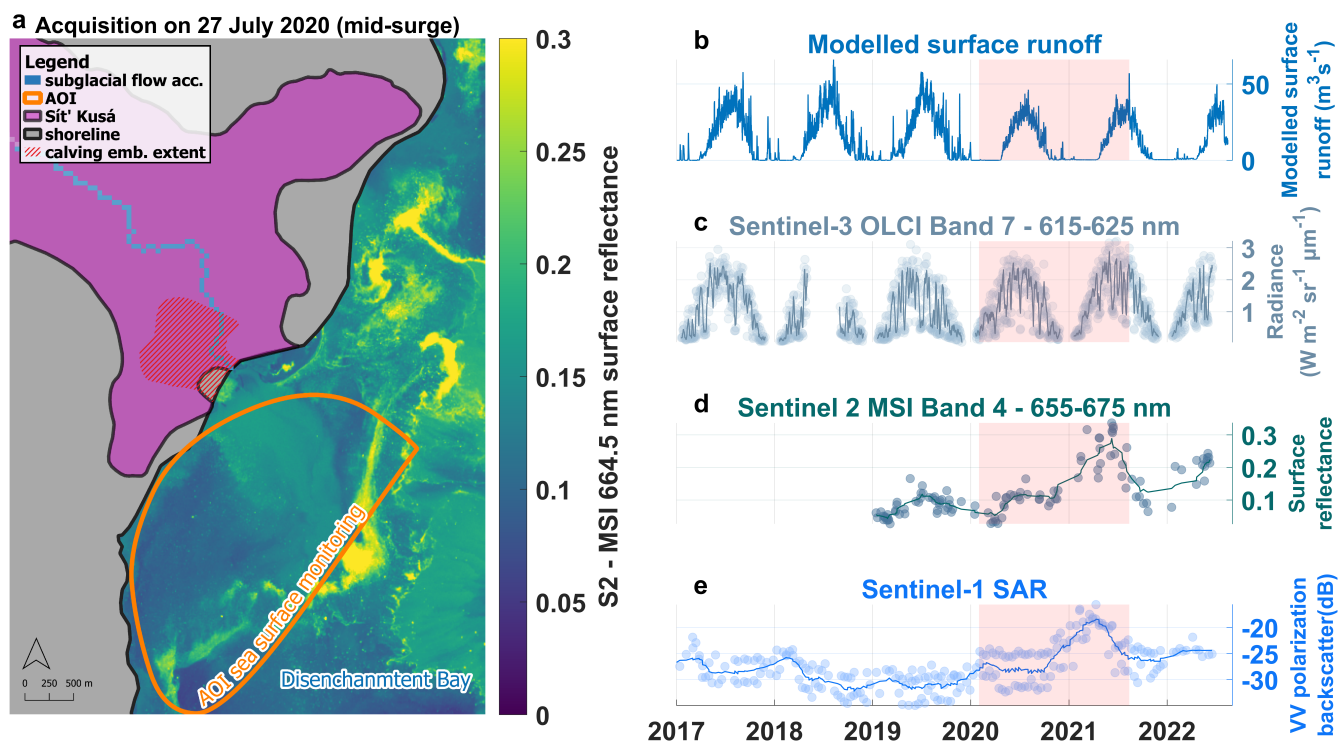


**Fig. 3.** a) False color showing surface reflectance in band 4 of Sentinel-2 MSI instrument. Image acquired on July 27<sup>th</sup> 2020, ~5 months after surge initiation and 13 months before surge termination. Sit' Kusá RGI outline shown in purple and shore shown in grey. Later in the surge the terminus advances entirely into the bay. Orange polygon shows area of interest over which observations are averaged. Blue pixels show hypothesized subglacial flow pathway based on flow accumulation analysis. b) Modelled surface runoff. c) Radiance in Sentinel-3 OLCI band 7. d) Surface reflectance in Sentinel-2 band 4. e) Sentinel-1 Synthetic Aperture Radar Ground Range Detected Vertical-Vertical-polarized back-scatter. Time-series show individual data points and a 10-point moving average.

237 when large volumes of meltwater are released as freshwater upwelling would push icebergs out of our defined  
 238 area of interest (Bartholomaus and others, 2013).

### 239 Surface Velocities

240 We include data from five Trimble Net R9 Global Positioning System (GPS) receivers and Septentrio  
 241 PolaNt-x MF antennas provided by EarthScope Consortium which were deployed and recovered on the ice  
 242 surface at various times and locations (Fig.1). We processed the data with the Canadian Spatial Reference  
 243 System Precise Point Positioning algorithm. We averaged the positions at daily intervals and differenced  
 244 consecutive positions to compute daily ice surface velocities. Surface velocities are not spatially uniform  
 245 throughout the surge (Liu and others, 2024), such that these point velocities cannot be spatially extrapo-  
 246 lated. Nevertheless, the records provide insight into velocity fluctuations at high temporal resolution. We  
 247 supplement the in situ velocity measurements with satellite-image derived velocity estimates made with

248 the open-source autoRIFT package (Lei and others, 2021). We include surface velocities in the upper  
249 trunk (15 km from the terminus) from pixel displacements derived from pairs of optical images (Sentinel-  
250 2 and Landsat-8) with date separations between 5 and 60 days and Synthetic Aperture Radar Imagery  
251 (Sentinel-1A and -1B) with date separations of 12 days (Liu and others, 2024).

## 252 RESULTS

253 We present time-series of the modelled surface runoff and seismic tremor (Fig.4a), of coherence and time-  
254 lags between tremor signals (Fig.4b), of glacier surface velocity (Fig.4c), and of water turbidity in front of  
255 the terminus (Fig.4d). The time-series start in late summer 2020, ~6 months after the start of the surge,  
256 and continue to August 2022, ~12 months after surge termination. The sections below describe these  
257 time-series in further detail.

### 258 Simulated Surface Runoff

259 The timing of the onset and end of surface runoff is relatively consistent from year to year in our study  
260 period, around 15 April and 15 October, respectively (Fig.4a). The highest runoff rates are generally  
261 reached around mid-June and persist until late August. The runoff during the 2021 melt season is not  
262 abnormally high (Fig.3b), with several spikes of  $\sim 37 \text{ m}^3\text{s}^{-1}$  occurring on 30 June and on 13-15 August  
263 which is the maximum runoff rate during the 2021 melt season.

### 264 Seismic Tremor Signal

265 The long term tremor signal shows high amplitude during the 2020 surge winter and during the 2021 melt  
266 season. A strong decrease in amplitude during the 2021-2022 winter is followed by renewed higher tremor  
267 amplitude during the 2022 melt season. There is a sudden but relatively small decrease in tremor amplitude  
268 ( $\sim -150 \text{ dB}$  to  $\sim -155 \text{ dB}$ ) in the glaciohydraulic tremor window in early October 2020, at the end of the  
269 melt season (Fig.4a, Fig.S1.2). However, tremor levels remain comparatively high throughout the winter of  
270 2020-2021 with small variations of  $\pm 2 \text{ dB}$  and a gradual increase coinciding with the onset of the 2021 melt  
271 season. The variability in glaciohydraulic tremor amplitude increases and remains high from June 2021  
272 until the end of our record (the standard deviation in the SE7 tremor signal between 15 September 2020 to  
273 1 June 2021 is 1.63 dB and between 1 June 2021 to 1 August 2022 the standard deviation is 7.30 dB). The  
274 13 August runoff event coincides with a strong spike in tremor, followed by a net drop in tremor amplitude

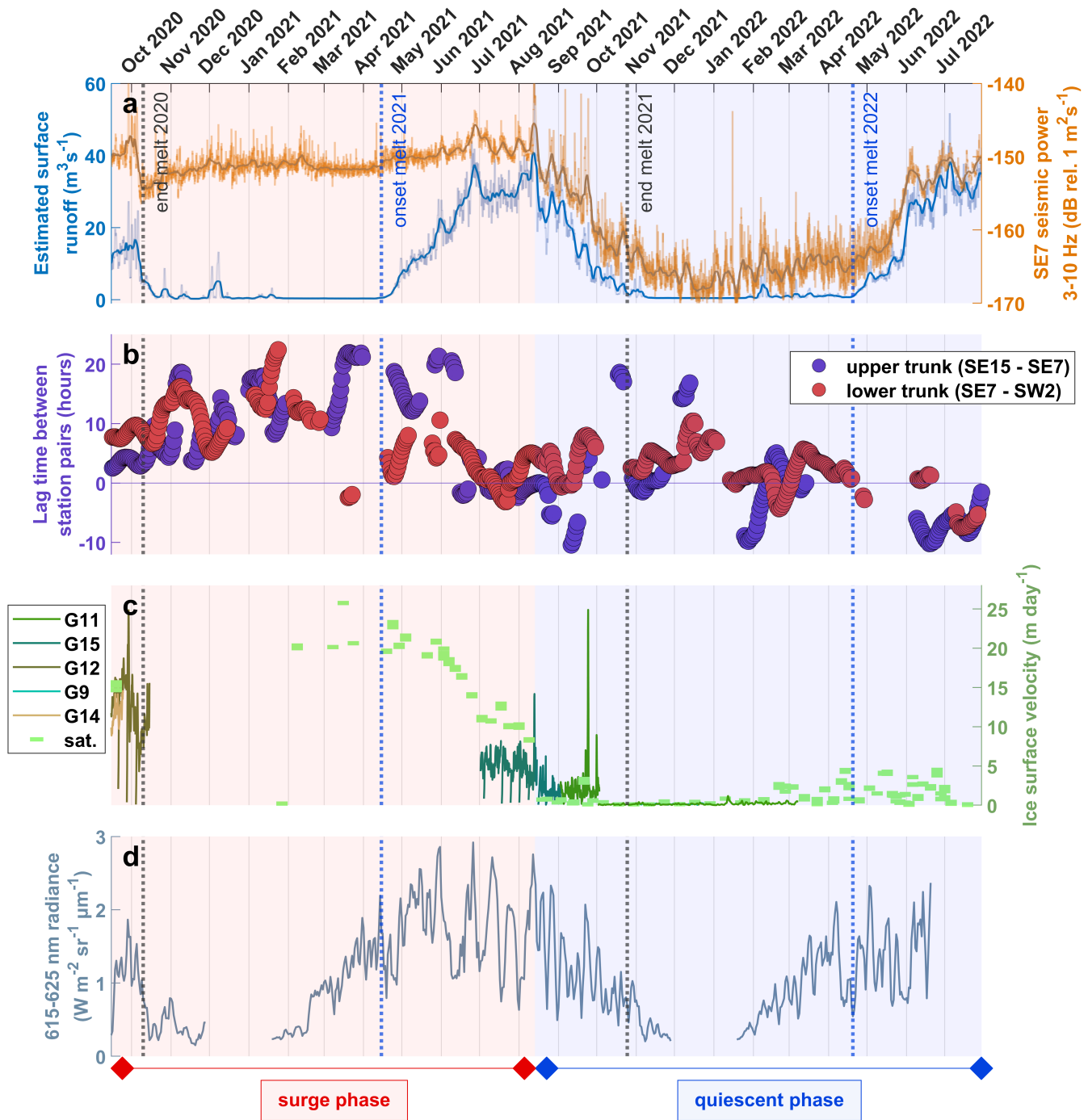


**Fig. 4.** a) Modelled estimate of surface runoff on Sít' Kusá at a location near SE7 (UTM zone 7, 571931 E, 6658040 N) and median seismic power recorded at SE7 in 3-10Hz frequency range. 5 day moving averages of plotted as thicker lines. b) Time-lags between glaciohydraulic tremor signals between station pairs SE15-SE7 and SE7-SW2. Only values with coherence above 0.7 are plotted. c) Surface velocities recorded at various on ice GPS receivers and through satellite image pairs. G12 and G9 overlap with G15 and G11 and are difficult to discern on the figure. d) Radiance recorded in Sentinel 3 OLCI band 7. Shaded area in the time-series show the extent of the 2020-2021 active phase.

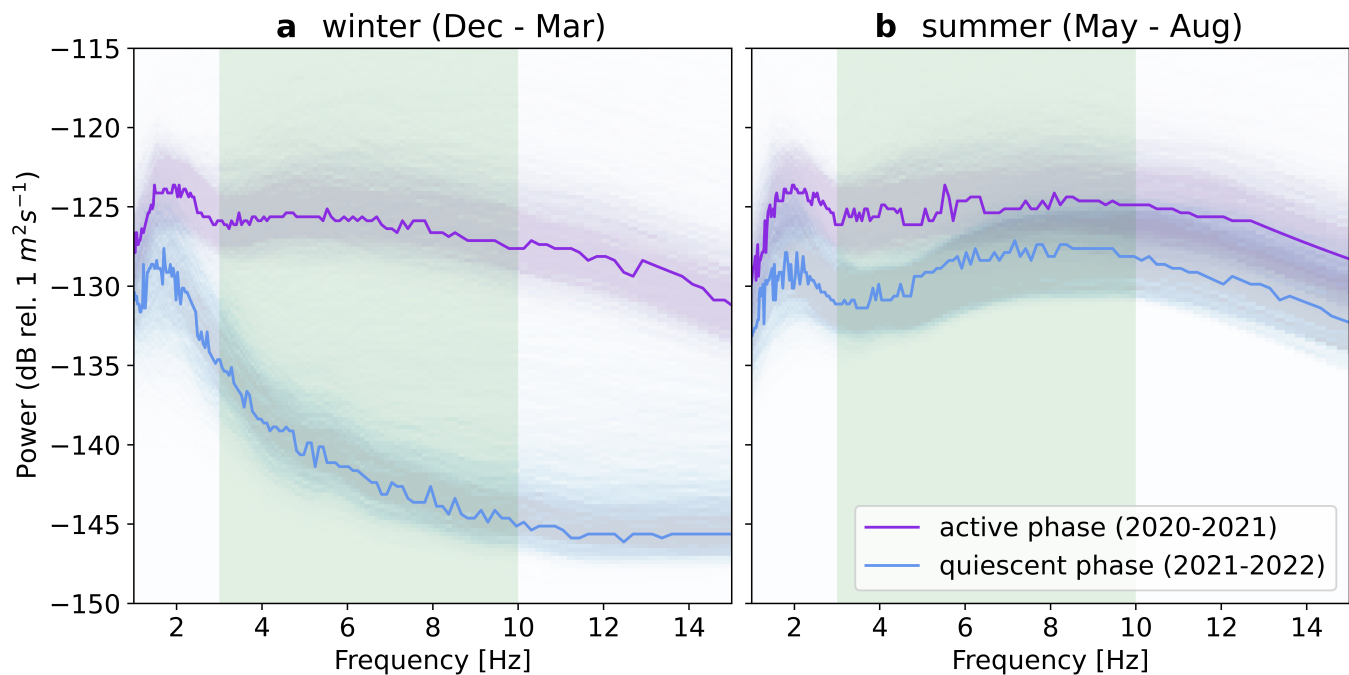


**Fig. 5.** Power spectral density functions (McNamara and Buland, 2004) with 50<sup>th</sup> percentile values plotted from seismic noise recorded at SE7 showing distribution and median power for time-periods a) in winter (1 December-1 March) and b) during the following melt season (1 May-1 August). Purple and blue lines differentiate between the active phase (winter 2020-2021 and summer 2021) and the subsequent quiescent phase (winter 2021-2022 and summer 2022). Green shading indicates frequency range within which we consider glaciohydraulic tremor.

275 relative to pre-termination levels ( $\sim -150$  dB to  $\sim -155$  dB). The tremor signal decreases from  $\sim -150$  dB to  
 276  $\sim -167$  dB between 15 August 2021 and 1 November 2021, closely mirroring the gradual decrease in surface  
 277 runoff from its summer maximum to the end of the melt season (Fig.4a, Fig.S4.2). During this period,  
 278 brief spikes in surface runoff coincide with spikes in the tremor signal. Tremor remains low ( $\sim -167$  dB)  
 279 throughout the winter but the signal continues to show variability of  $\pm 5$  dB that appears unforced by  
 280 surface runoff. After the onset of melt in 2022, the tremor amplitude increases to  $\sim -153$  dB, about 3 dB  
 281 below levels recorded during the surge. The rate of increase closely follows the rate of increase of surface  
 282 runoff with a more gradual increase between 15 April and 15 May followed by a more rapid rise between  
 283 15 May and 5 June. Seasonal median noise levels recorded at SE7 (Fig.5) also indicate that melt season  
 284 tremor amplitude is relatively similar during the surge (May-Aug. 2021) and post-surge (May-Aug. 2022)  
 285 but that winter tremor amplitudes are much higher during the surge (Dec. 2020-Mar. 2021) than after the  
 286 surge (Dec. 2021-Mar. 2022).

## 287 **Lags between seismic tremor time-series**

288 There is high coherence between seismic tremor signals within both the SE15-SE7 and SE7-SW2 station  
289 pairs during the surge with brief ( $\sim 4$  weeks) disruptions in coherence for the lower trunk during March  
290 and early April 2021 (Fig.4b, Fig.S5.2). Coherence in the upper trunk frequently breaks down after surge  
291 termination. In the lower trunk, coherence is maintained during the 2021-2022 winter but largely absent  
292 during the 2022 melt season.

293 The time-lags between coherent tremor signals observed at SE7 and SW2 (Fig.4b), vary between  $\sim 8$   
294 and 20 hours from August 2020 to April 2021, with a faint increasing trend. The disruptions in coherence  
295 for the lower trunk occurring in March-April are accompanied by a brief period of negative time-lags ( $\sim -3$   
296 hours). Meanwhile, time-lags in the upper trunk show a more clear but non-monotonic increasing trend  
297 from  $\sim 2$  hours during the 2020 melt season to  $\sim 20$  hours by April 2021. Time-lags in both the upper and  
298 lower trunk decrease between April 2021 and July 2021 and vary between -10 hours and 10 hours during  
299 the second half of the 2021 melt season.

300 After surge termination, limited moments of high coherence in the upper trunk are marked by a wide  
301 range in time-lags with values ranging between -10 hours and 20 hours. Lower trunk values vary between  
302  $\sim -1$  hour and  $\sim 10$  hours for the remainder of the melt season and during early winter. Between January  
303 and April 2022, we observe time-lags in the lower trunk that range between -5 hours and 10 hours. Despite  
304 these variations, the time-lags during the 2021-2022 winter are consistently lower than those during the  
305 2020-2021 winter for both the upper and lower trunk.

## 306 **Remote Sensing Time-series**

307 There is a consistent seasonal signal in the radiance values recorded with Sentinel-3 OLCI Band 7 (615-625  
308 nm), with turbidity decreasing shortly after the end of the melt season and increasing around mid-February  
309 of each year (including during the 2020 and 2021 surge winters),  $\sim 2$  months before the onset of the melt  
310 season (Fig.4d). This seasonal signal is also present in the temporal evolution of the Sentinel-2 MSI surface  
311 reflectance although the latter record is limited in temporal resolution. The Sentinel-1 record shows a  
312 seasonal peak in back-scattering that precedes the peaks in the other two signals. Both the Sentinel-1 and  
313 Sentinel-2 records show a spike during the first half of 2021, when calving rates are maximal (Fig.S2.1).  
314 In the higher temporal resolution Sentinel-3 signal, yearly average radiance is only slightly higher in 2021  
315 ( $1.25 \text{ W m}^{-1} \text{ sr}^{-1} \mu\text{m}^{-1}$ ) than in 2019 ( $0.91 \text{ W m}^{-1} \text{ sr}^{-1} \mu\text{m}^{-1}$ ) and 2020 ( $1.04 \text{ W m}^{-1} \text{ sr}^{-1} \mu\text{m}^{-1}$ ). The total



316 amplitude of these variations is  $\sim 0.34 \text{ W m}^{-1} \text{ sr}^{-1} \mu\text{m}^{-1}$  relative to an average seasonal standard deviation  
317 of  $0.76 \text{ W m}^{-1} \text{ sr}^{-1} \mu\text{m}^{-1}$  (standard deviation of  $0.14 \text{ W m}^{-1} \text{ sr}^{-1} \mu\text{m}^{-1}$  between seasons). Finally, we do not  
318 observe abnormal peaks or steps in turbidity during the 2021 melt season.

### 319 **Surface velocities**

320 Fig.4c shows the evolution of surface velocities from 2020 to 2022 recorded through GPS measurements  
321 and displacement observed in satellite imagery (Liu and others, 2024). Velocity measured at the G12 GPS  
322 station decreases from  $\sim 20 \text{ m d}^{-1}$  to  $\sim 10 \text{ m d}^{-1}$  in early October 2020, coinciding with the end of the melt  
323 season. However, ice velocities increase again within a few days and the satellite record indicates velocities  
324 reached  $\sim 20 \text{ m d}^{-1}$  by mid-February. The velocities derived from satellite observations further indicate a  
325 gradual slowdown from nearly  $\sim 20 \text{ m d}^{-1}$  in June 2021 to  $\sim 10 \text{ m d}^{-1}$  in mid-August 2021. Thirteen August  
326 2021 is marked by a brief peak in ice velocities to  $\sim 15 \text{ m d}^{-1}$  followed by a sudden decrease to velocities  
327 generally below  $5 \text{ m d}^{-1}$ .

328 It is noteworthy here that there are high amplitude ( $\pm 5 \text{ m d}^{-1}$ ) variations in surface velocity during  
329 the surge on timescales of 1 to  $\sim 10$  days that are captured by the GPS record but missed in the satellite  
330 derived velocity estimates. The amplitude of this variability is reduced, but remains present, at the end  
331 of the 2021 melt season during which surge termination occurs. We note two very short lived spikes to  
332 over  $10 \text{ m d}^{-1}$  in late September 2021 in the G11 record. Velocities remain very low ( $\sim 1 \text{ m d}^{-1}$ ) during the  
333 2021-2022 fall to early winter and increase to  $\sim 3 \text{ m d}^{-1}$  from February 2022 until early July 2022. The  
334 velocities then decrease to  $\sim 1 \text{ m d}^{-1}$  by mid July 2022.

## 335 **DISCUSSION: SIGNAL ATTRIBUTION**

336 This work relies on a wide range of observation sources that complement each other towards a picture of ice  
337 flow and subglacial drainage behavior. Many of the time-series are proxies for the glaciological quantities  
338 we are interested in. We devote this initial part of the discussion to an assessment of the reliability of, and  
339 possible caveats to, our observations.

### 340 **Relation between modelled surface melt and surface runoff**

341 The energy balance firn model used to estimate surface runoff has several free parameters, notably including  
342 the rain to snow transition temperature, the elevation dependent precipitation gradient, and broadband



343 albedo values (e.g. van Pelt and Oerlemans, 2012). Additionally, energy balance models are strongly  
344 dependent on the quality of meteorological input data. To assess the accuracy of our model estimates we  
345 compare the modelled surface elevation change on Sít' Kusá at several dates with five digital elevation  
346 models derived from Worldview images acquired during the 2022 melt season. We find a correlation  
347 coefficient of 0.88 and a root mean squared error of 1.3 m (Text S3b). We tolerate this error extent for  
348 our purposes as we focus on the relative variation in surface runoff rather than absolute surface mass  
349 balance estimates. The advantage of including a consideration of runoff buffering in the snow and firn pack  
350 outweighs the simplicity of a positive degree day approach.

### 351 **Relation between surface runoff and subglacial water delivery to the glacier bed**

352 We observe that peaks in modelled surface runoff consistently coincide with spikes in seismic tremor power  
353 (Fig.4, Fig.S4.2). Several studies have noted how increases in tensile stresses and extensive crevassing  
354 during surges promotes penetration of surface melt to the bed (Dunse and others, 2015; Sevestre and  
355 others, 2018; Gong and others, 2018). Our data covers broadly the latter two thirds of the surge: extensive  
356 crevassing was already present in August 2020 at the time of sensor installation, allowing a direct and  
357 widespread connection between the glacier surface and the bed. Supraglacial water routing would have  
358 been extremely limited by the crevassed nature of the surface during the surge (Fig. 6, Text S3c). Figures  
359 4 and 8 provide perspective on the short term response of ice velocity to changes in surface melt supply.  
360 An example here is the peak in surface melt driven by a rainstorm on 13 August 2021 that resulted in a  
361 brief threefold increase in ice velocity (Fig.4). Such a direct response of velocity to water supply echoes  
362 observations made on non surge type alpine glaciers (e.g. Iken and Truffer, 1997; Bartholomaus and others,  
363 2008), and shows that volumes of surface melt contributions to the subglacial water budget are sufficient  
364 to impact the system. Thus, while delivery of surface melt to the bed might still be lagged by several hours  
365 relative to estimated runoff time, we take modeled surface runoff as the best available proxy for water  
366 delivery to the glacier bed.

### 367 **Relation between seismic tremor and subglacial water flow**

368 As with surface streams, the mechanism driving ground motion in subglacial conduits is thought to be a  
369 combination of the drag between turbulent water flow and conduit roughness and the rolling and saltation  
370 of sediment within the conduit (e.g. Tsai and others, 2012; Gimbert and others, 2016). As a result, the



**Fig. 6.** Photo of the glacier surface taken on 8 September 2020, ~10 km from the terminus along the main trunk of Síť Kusá, looking southeast towards the terminus. Inset shows location photo was taken. Photo by T.C. Bartholomaus.

371 amplitude of the seismic tremor varies with both the water velocity and the sediment flux through the  
372 conduit, with the respective contributions of these processes difficult to disentangle (Gimbert and others,  
373 2014). Understanding the drivers of seismic noise produced in streams remains an active field of study  
374 (e.g. Bakker and others, 2020) but previous work has shown that useful information on subglacial water  
375 flow can be derived from seismic tremor by neglecting contributions from sediment motion (e.g. Nanni and  
376 others, 2020, 2022) or by remaining agnostic regarding the exact source mechanism (e.g. Bartholomaeus  
377 and others, 2015).

378 A possible alternate source of tremor is frictional stick-slip tremor at the ice-bed interface (Lipovsky and  
379 Dunham, 2017), echoing behavior observed along subduction zones (e.g. Shelly and others, 2006). Podolskiy  
380 and others (2021) find tidally modulated changes in seismic noise within the 3-14 Hz frequency range that  
381 are best explained as sourced from changes in basal sliding speed along a glacier bed/till interface. Stick-  
382 slip tremor, correlated with surface motion, has also been identified using geophones installed within 50  
383 m of the glacier bed (Köpfler and others, 2022). There, the spectral content (chiefly  $> 10$  Hz) was tightly  
384 banded and varied with fluctuating basal water pressures. If the tremor signal observed on Sít' Kusá was  
385 modulated by sliding rates, we would expect the correlation between tremor and sliding to be most clear in  
386 the absence of strong glaciohydraulic tremor. Contemporaneous recordings of GNSS-based surface velocity  
387 at G14 and seismic tremor at the adjacent SW14 at the close of the melt season (from 1 October 2020 to  
388 15 November 2020) do not reveal a significant correlation between the two time-series ( $r = 0.17$ ; Fig.S4.1).  
389 We also do not identify any shifts in frequency content (i.e., gliding) within the tremor we record that  
390 would be consistent with stick-slip tremor (Köpfler and others, 2022; Lipovsky and Dunham, 2017).

391 Instead, we record clear increases in tremor amplitude during the melt season (Fig.4a,5) and find good  
392 agreement between variations in modelled surface runoff and seismic tremor (Fig.4a;  $r=0.72$  for the 2021  
393 melt season, 15 April to 15 October 2021; and  $r=0.52$  for the whole record), as reported at other glaciers  
394 (Bartholomaeus and others, 2015; Vore and others, 2019). Even at the close of the melt season, with  
395 waning water influx, the correlation between tremor and melt is far stronger than that between tremor  
396 and ice flow velocity ( $r = 0.69$  as compared with  $r = 0.17$ ; Fig.S4.1). Furthermore, the tremor time-  
397 series at upglacier and downglacier stations reveal coherent variations in power that lag each other and  
398 propagate downglacier with celerities expected for water flow (see next section). As such, we infer that the  
399 amplitude of the tremor signal is driven primarily by the hydraulics of subglacial waterways beneath Sít'  
400 Kusá and scales with water velocity through these waterways (Bartholomaeus and others, 2015). We have

401 not attempted to resolve which hydraulic process(es) may specifically control variations in tremor power  
402 at Sít' Kusá—whether turbulent water flow or sediment transport—and expect that stick-slip tremor may  
403 be present within our time-series at some level. However, from the preponderance of evidence we interpret  
404 seismic tremor variations as a proxy for subglacial water flow.

## 405 **Relation between seismic tremor time-lags and subglacial drainage system** 406 **configuration**

407 The time-lags between glaciohydraulic tremor recorded at different locations along the glacier require careful  
408 interpretation. Following Grinsted and others (2004), we compute time-lags only when there is a high level  
409 of coherence between the seismic tremor time-series. Despite their similarity, the source mechanisms and  
410 source locations of the tremor time-series must be independent: the time-lags between the time-series are  
411 on the order of hours, which is much longer than if the tremor time-series recorded at each station were  
412 sourced by a single process and the lags were caused by travel times of seismic waves. Glacio-hydraulic  
413 tremor generally attenuates to undetectable levels within  $\sim 3$  km (Bartholomaus and others, 2015; Vore and  
414 others, 2019), leading us to expect that the recorded tremor was generally sourced in close proximity to  
415 the respective receivers. We focus on the SE15-SE7 and SE7-SW2 station pairs to maximize the distance  
416 between likely tremor source locations.

417 While Fig.2 illustrates a straight-forward time lag signal extracted from a portion of the seismic record,  
418 the full time-series show more complex behavior. Notably, the occurrence of negative lags suggests the  
419 tremor time-series recorded at the downglacier station can be ahead of the tremor recorded at the up-  
420 glacier station. A closer inspection of the tremor time-series during key time-periods provides some insight  
421 into the various situations producing these time-lags between SE15 and SE7 (Fig.7), as described below.  
422 Supplementary material Text S5 provides a similar evaluation for SE7-SW2 along with the full time-  
423 frequency plots of the time-lags between both station pairs (Fig.S5.3, Fig.S5.4).

424 During March 2021, in the absence of surface runoff, tremor at SE15 shows a remarkable pattern  
425 including a gradual increase of  $\sim 1$  dB lasting at least several days followed by a sudden  $\sim 4$  dB spike in  
426 tremor that lasts  $\sim 48$  hours. This pattern is mimicked at SE7  $\sim 22$  hours later and with lower amplitude  
427 ( $\sim 2$  dB peaks). If the seismic tremor is indeed predominantly hydraulic in origin, this similar tremor  
428 pattern strongly hints at a pulse in water velocities that travels downglacier. These time-lags are some of  
429 the longest in our record and we note a lack of coherence between signals before and after the highlighted

430 period, suggesting a lack of connection in the drainage system during those surrounding time periods.  
431 The pulse-like pattern within the tremor time-series could be the signature of water being released out  
432 of overwinter storage (Liu and others, 2024), likely under high pressure, as this could generate the strong  
433 increases in tremor power (e.g. Gimbert and others, 2016; Nanni and others, 2021). Such events would  
434 likely have an expression on the ice surface, including a brief speedup and surface uplift (e.g. Iken and  
435 Bindshadler, 1986). Unfortunately we do not have surface GPS measurements during this time period.  
436 Echoes of similar behavior are present sporadically in our record (Text S5) but none are as clear as shown  
437 here.

438 During early February 2022, we find evidence of a likely similarly poorly drained subglacial environment.  
439 Short lived and strong pulses ( $> 5\text{dB}$ ) in tremor recorded at SE15 do not materialise at SE7. Furthermore,  
440 the tremor pulses that do exist in the records of both seismic stations occur at SE7 5 to 10 hours earlier  
441 than at SE15. The travel of tremor pulses in the up-glacier direction might be caused by a pressurized  
442 drainage system that “backs-up” water, where the drainage system cannot accommodate the water influx  
443 and forces a water pressure pulse to migrate up-glacier (e.g. Barrett and Collins, 1997; Bartholomaus and  
444 others, 2008). Another example of this suspected behavior is shown in Fig.S5.2. The behavior changes  
445 after 5-10 February 2022, a brief warm period during which there is up to  $10\text{ m s}^{-1}$  of surface runoff on  
446 the glacier, an infrequent event during the winter-time. Both tremor signals respond to the water supply  
447 and the SE15 signal leads the SE7 signal afterwards, suggesting that perhaps the additional water led to  
448 an increase in drainage efficiency.

449 During June and July 2021, there is a transition from  $\sim 20$  hour lags to  $\sim 5$  hour lags. Both tremor  
450 signals show daily fluctuations that follow the diurnal melt cycle and time-lags at a one day period are  
451 close to zero. This suggests a well connected system where the tremor signals are a combined product of  
452 subglacial water flow downglacier and distributed water input from surface runoff. Interestingly, the long  
453 period ( $> 5$  day) increase in both tremor signals, forced by a long term increase in surface runoff, occurs  
454 earlier at SE7 than at SE15. This difference in timing is likely caused by differences in snow cover thickness  
455 as a thinner snowpack would have a lower capacity to retain surface melt (e.g. van Pelt and others, 2016),  
456 leading meltwater reach the subglacial environment more quickly lower on the glacier.

457 Similar behavior is more obvious during June and July 2022, with the SE7 signal consistently leading  
458 the SE15 signal. Both tremor time-series show diurnal variability that follows the runoff signal but the  
459 amplitude of these oscillations is higher for SE7 than for SE15. Occasional peaks in SE15 tremor do not

460 materialise in the SE7 record. We suggest that during June and July 2022 the time-lag signal is dominated  
461 by distributed surface water supply to the subglacial system: localized runoff quickly penetrates to the  
462 glacier bed and affects the local tremor signal. When we detect negative lags, the effect of the distributed  
463 water supply on the drainage system is strong enough to “drown out” the tremor generated by downglacier  
464 water transport. This would be aided by poor along-flow connection within the drainage system but could  
465 be caused by very high surface runoff rates. There are frequent examples of this occurring on diurnal  
466 timescales (Fig.7, Fig.S5.2).

467 The above examples, along with further examples and the full time lag time-series shown in Fig.S5.3  
468 and Fig.S5.4, shape the interpretation of the time lag time-series. Strongly positive lags (~5-25 hours) hint  
469 at connected but slow moving subglacial drainage in the downglacier direction. Slightly positive lags point  
470 at a connected drainage system with some efficient component through which water moves downglacier  
471 quickly. Negative lags are often driven by distributed surface runoff supply but could also reflect up-glacier  
472 migration of pressure pulses in a connected but poorly draining system. Finally, negative lags that persist  
473 for longer periods of time during the melt season are most likely driven by surface melt reaching the  
474 subglacial environment in a distributed manner.

475 We note that the time-lags are less varied and more consistently positive during the surge. Following  
476 our interpretation of the time-lags outlined above, this implies that the drainage system is more frequently  
477 connected and downglacier motion of water or pressure pulses is more prevalent during the surge than after  
478 termination. Nevertheless, the disruption in coherence during the late winter of 2021 shows that there is a  
479 continued seasonal evolution, including a poorly connected phase, in the drainage system during the surge.

## 480 **Relation between remote sensing time-series and fjord conditions**

481 The seasonal fluctuation in the Sentinel-3 and Sentinel-2 signals (Fig.3) provides confidence that the longer  
482 term changes in the recorded radiance and reflectance are driven by the release of meltwater (e.g. McGrath  
483 and others, 2010). The Sentinel-1 signal reflects the back-scattering at the surface, which is largely driven  
484 by the presence of small icebergs at the water surface (Benn and others, 2019b). Our observations reflect  
485 this as the amount of back-scattering strongly increases in October of 2020. This coincides with the time  
486 at which Sít' Kusá has covered its sediment shoal and is advancing into Disenchantment Bay, promoting  
487 more consistent calving (Liu and others, 2024). The Sentinel-2 signal shows a similar increase in late 2020  
488 to levels similar to those recorded for the permanently iceberg filled water in front of Sít' Tlein (Hubbard



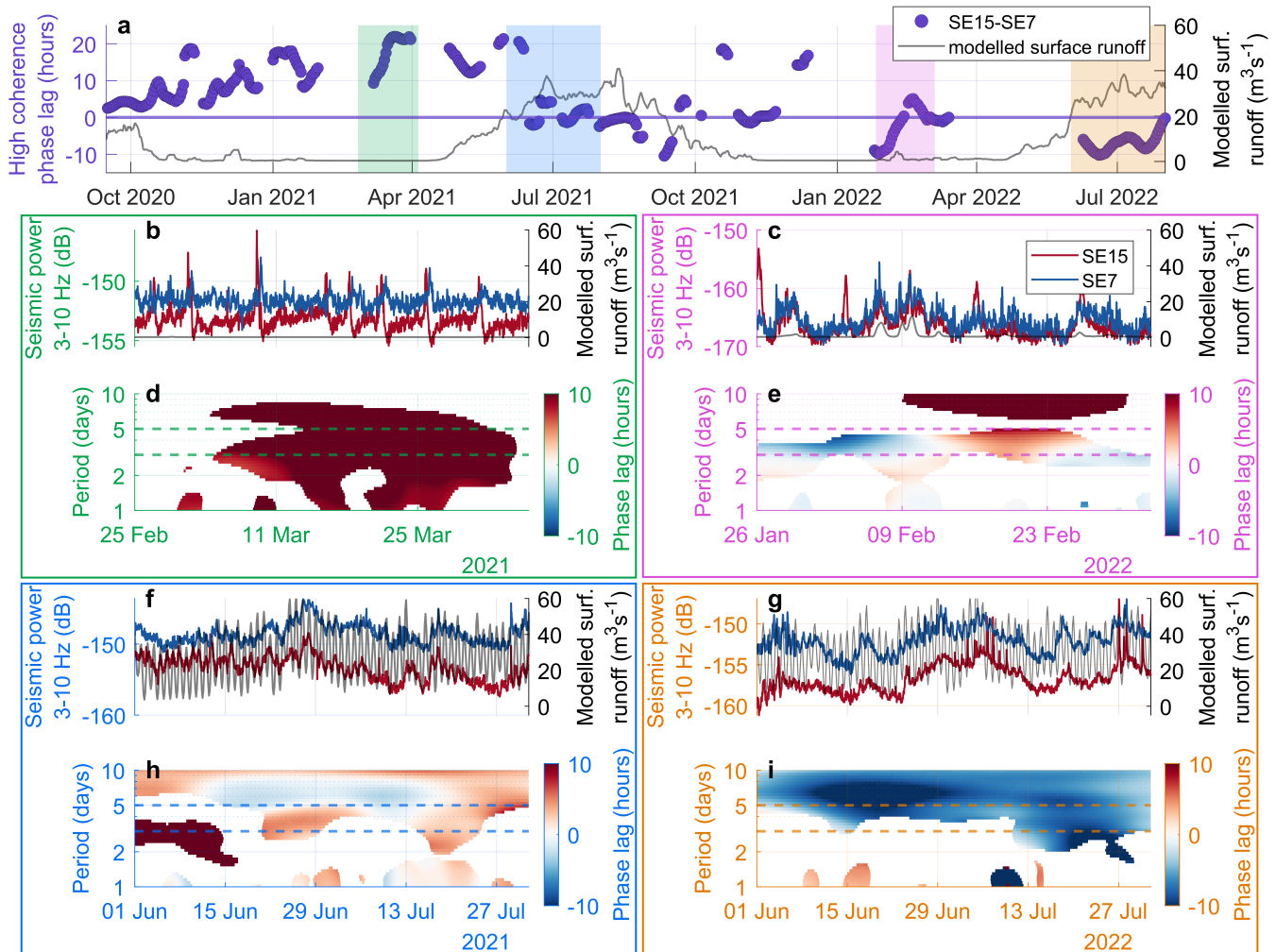


**Fig. 7.** a) Three to five day period phase lags between seismic tremor signals recorded at SE15 and SE7 shown on left hand axis in purple. Modelled surface runoff shown in grey on right hand axis. b)-i) Detail views of four highlighted periods. Each colored frame of two panels shows the two tremor signals and the modelled melt signal in the upper panels (b,c,c,g) along with their associated time/frequency lag plots in the lower panels (d,e,f,i).



489 Glacier), suggesting that the surface reflectance is also affected by the increase in icebergs in the bay. The  
490 Sentinel-3 signal seems less affected by iceberg presence, which we suspect might be due to a combination  
491 of higher spectral resolution and lower spatial resolution relative to Sentinel-2.

492 The Sentinel-1 back-scattering intensity is maximal early in the melt season and decreases during  
493 the summer as the turbidity derived from Sentinel-3 increases (Fig.3), consistent with the suggestion  
494 that increased subglacial discharge pushes away icebergs from the area of interest. This pattern gives us  
495 confidence that the Sentinel-3 OLCI band 7 time-series capture changes in water turbidity in front of the  
496 Sít' Kusá terminus and is a plausible proxy observation for the relative intensity of subglacial water release  
497 at the terminus. While our observations do not provide a definitive measure of sub-aqueous discharge  
498 volumes, they are mutually consistent and we have good confidence that they reflect the relative variability  
499 in sub-aqueous frontal discharge. The close proximity of the tidewater terminus of Sít' Tlein likely affects  
500 our observations to some extent, as shown by seasonality in the inferred iceberg production before the Sít'  
501 Kusá terminus reaches the ocean. A similar analysis for an area chosen to capture discharge from the Sít'  
502 Tlein terminus shows commonalities with the data recorded for the Sít' Kusá terminus but also notable  
503 differences (Fig.S6.1). We have chosen the area of interest as far removed from the Sít' Tlein terminus as  
504 possible (Fig1,3a) and thus expect the signals to be dominated by changes at the Sít' Kusá terminus.

## 505 **DISCUSSION: SIGNAL INTERPRETATION**

506 In this section we aim to disentangle the behavior of the subglacial drainage system and how it affects ice  
507 dynamics through the interpretation of our various time-series. Each subsection is titled with an assertion  
508 that we subsequently support by our observations.

### 509 **An efficient component of the subglacial drainage system exists intermittently prior** 510 **to surge termination**

511 Our observations show that tremor-generating glaciohydraulic sources exist prior to surge termination at  
512 least at several locations along the main trunk of Sít' Kusá (Fig.S1.1, Fig.S5.5): we find tremor during  
513 the mid-surge summer that has similar power to that of the quiescent summer and the tremor power of  
514 the mid-surge winter is within several dB of summer levels (cf. quiescent winter tremor which is ~15  
515 dB lower than mid-surge winter). Additionally, the tremor spectral pattern remains consistent between  
516 hydraulically-active summers and the active phase winter (Fig.5), suggesting similar source mechanisms.

517 Previous work widely attributes such tremor to turbulent flow and sediment transport through a channelized  
518 subglacial drainage system (e.g. Bartholomaus and others, 2015; Gimbert and others, 2016; Nanni and  
519 others, 2020; Lindner and others, 2020). Furthermore, Nanni and others (2021) inferred that inefficient,  
520 broadly distributed, linked cavities can also produce detectable hydraulic tremor, albeit with power 20 dB  
521 less than that of mid-summer (Gimbert and others, 2021). However, the mid-surge 2020-2021 winter tremor  
522 we record remains within  $\sim 5$  dB of peak power (Fig.4a), which is a much smaller gap than the change  
523 in tremor power associated with the transition from linked cavities to channelized drainage on Argentière  
524 Glacier (Nanni and others, 2020, 2021).

525 These tremor generating locations have hydrologic connections to the surface (Fig.4a), as the tremor  
526 power consistently shows spikes that coincide with spikes in modelled surface runoff (Fig.4a). Additionally,  
527 these tremor generating locations are connected in the along flow direction, as we can detect lagged coher-  
528 ence between the tremor signal observed at various seismic stations (Fig.4b). We do not know the precise  
529 location of the tremor sources and thus cannot infer the exact travel distance of the water velocity pulse  
530 through the subglacial drainage system. Nevertheless, the source locations are almost certainly within  $\pm 3$   
531 km of the centerline distance between station pairs, meaning  $\sim 8.2$  km  $\pm 3$  km for SE15-SE7 and 5 km  $\pm 3$   
532 km for SE7-SW2. Despite the large uncertainties, these distances are within the same order of magnitude  
533 as those used for dye tracing experiments on Variegated Glacier in Kamb and others (1985) (8 km and  
534 10 km, their Fig.11). Our time-lags are universally below 25 hours; and the median positive time-lag for  
535 SE15-SE7 is 8.5 hours (Fig.4b) over the whole record and 9.4 hours when computed for just the surge  
536 phase (prior to 15 August 2021). These values are relatively close to those that Kamb and others (1985)  
537 attribute to post-surge efficient drainage (main dye concentration peak after  $\sim 4$  hours) and shorter than  
538 those found for the surge phase linked cavity system on Variegated Glacier (first dye concentration peak  
539 after  $\sim 50$  hours).

540 The upper range of the time-lags we observe (20-25 hours) and the detailed inspection of the lags in  
541 Fig.7 show that there are moments of inefficient, or disrupted drainage during the surge, notably from 1  
542 March to 15 April 2021 and during July 2021 (Fig.4b). However, considerable time periods of the surge  
543 with short time-lags and the absence of changes in the tremor frequency content lead us to suggest that  
544 there is at least intermittent efficient water transport occurring in an along flow component of the drainage  
545 system prior to surge termination.

546 This component is frequently present throughout the lower trunk of the glacier from September 2020

547 to April 2022 and in the upper trunk at least from September 2020 to October 2021. However, we cannot  
548 fully ascertain how prevalent the efficient components are spatially. It is possible and perhaps even likely  
549 that the tremor generating components of the subglacial drainage system do not coincide spatially with  
550 the area(s) of the glacier base regulating ice velocities or surge propagation.

551 The absence of coherent tremor variations in the upper trunk between October 2021 and August  
552 2022, and between April 2022 and August 2022 suggests that the subglacial drainage system is gradually  
553 disconnecting during the winter after surge termination. This is in line with the lower tremor amplitude  
554 during that period, as lower basal water volumes and slower water flow would allow for creep closure to  
555 gradually close off waterways and reduce the connectivity of the drainage system (e.g. Hart and others,  
556 2022).

### 557 **Subglacial water-flow continues during the surge winter**

558 A comparison of the power spectral density probability for the winter (December-March) and summer  
559 seasons (May-August) (Fig.5) shows that the median spectral power across the glaciohydraulic tremor  
560 frequency range is similar to but slightly lower during the post surge melt season compared to the surge  
561 melt season (Fig.5b). Both spectra have a similar shape, suggesting that there is a stable and consistent  
562 seismic source process (Gimbert and others, 2014) and further hinting that the subglacial hydrological  
563 systems during the summer of 2021 and 2022 are comparable in behavior. Meanwhile, median spectral  
564 power is considerably lower during the post surge winter compared to the active phase winter (Fig.5a). A  
565 second notable difference between the two winters in our record lies in the time-lags. The surge winter is  
566 marked by relatively consistent positive lags that reflect a connected drainage system where most seismic  
567 noise is produced by water or pressure pulses that move downglacier (Fig.4b,7). The 2021-2022 post surge  
568 winter sees less consistent coherence and much more variable lags (Fig.4b). This behavior points to a less  
569 connected system where distributed inputs from surface melt are relatively more important (Fig.7).

570 Together, our interpretation of the time-lags and the higher noise levels suggest that the drainage  
571 system during the 2020-2021 winter is “higher volume” than during the 2021-2022 winter. This winter  
572 volume is likely considerably lower than melt-season values, as there are disruptions in drainage during  
573 late winter 2021 (Fig.4b, Text S5) and bay turbidity decreases during the fall of 2020, in a similar pattern  
574 to other years (Fig.4d). Nevertheless, some continued base level of water availability during the winter  
575 would allow the drainage system to remain more connected and explain the higher tremor levels observed

576 in 2020-2021. In the absence of water supply from surface runoff, water might be sourced from sub- or  
577 englacial reservoirs. Such overwinter storage likely occurs annually on Sít' Kusá (Liu and others, 2024)  
578 and has been suggested to play a role in the surge mechanism on other Alaskan glaciers (Humphrey and  
579 Raymond, 1994; Lingle and Fatland, 2003; Barrett and others, 2008; Zhan, 2019; Hart and others, 2022).  
580 Additionally, water could be sourced through strain heating and basal melt (Benn and others, 2019a). Our  
581 interpretation of a “high water-volume” drainage system during the surge and “low water volume” drainage  
582 system post-surge is also consistent with the enthalpy based model of surging, where surge termination is  
583 driven by the draining of the glacier base (Benn and others, 2019a, 2022).

### 584 **Indistinguishable change in frontal discharge before and after the surge**

585 The seasonal cycle contained in the Sentinel-3 record seems largely unchanged throughout Sít' Kusá's  
586 surge cycle (Fig.3, 4e). The Sentinel-2 surface reflectance does see a spike starting in October 2020, but as  
587 discussed earlier its similarity to the Sentinel-1 signal suggests that it is driven by iceberg presence rather  
588 than water turbidity (Fig.3). As such, our indirect observations do not point to a significant disruption in  
589 frontal discharge during the surge build up or during the active phase and while the seasonally averaged  
590 turbidity in the bay is slightly higher in 2021 relative to 2019, we are unable to observe a sudden single  
591 abnormally high-volume discharge event during the 2021 melt season (Fig.4d).

592 Previous work frequently notes retention of water below the glacier during the active phase (Clarke and  
593 others, 1984; Lingle and Fatland, 2003), while termination coincides with release of large volumes of water  
594 from the subglacial environment (e.g. Kamb and others, 1985; Benn and others, 2019b). We are unaware  
595 of descriptions of prior Alaskan surge terminations specifically noting an absence of abrupt water releases  
596 from the terminus.

597 While it is possible that our proxy record simply missed a spike due to cloudy conditions, the bay  
598 turbidity record is consistent with our earlier interpretations of the drainage system. Each year, turbidity  
599 in front of the terminus starts increasing before the spring onset of surface runoff (Fig.4d, 3). This early  
600 increase might be associated with the frontal release of water stored overwinter, linked to the annual early  
601 spring speedups described in Liu and others (2024). The apparent lack of disruption in frontal discharge  
602 during the surge is also consistent with our interpretation that efficient drainage occurs intermittently dur-  
603 ing the surge. The absence of a single major water release event could suggest a rather gradual termination  
604 of the surge on Sít' Kusá, which we discuss further in the next section.

605 **Short term velocity fluctuations modulated by subglacial drainage overlay gradual**  
606 **surge termination**

607 Here we focus on the various time-series related to hydrology for the 2021 melt season that marks surge  
608 termination (Fig.8). Lags in the upper trunk decrease from 20 hours in early June to alternating slightly  
609 negative and positive five hour lags, which we have interpreted earlier to reflect an intermittently connected  
610 and efficient drainage system component with significant contributions from distributed surface melt. From  
611 mid-June to early-July, the tremor pulse velocities in the lower trunk gradually decrease from >5 hours  
612 to ~1 hour. The lag time decrease coincides with a gradual decrease in ice surface velocities from >15 m  
613 d<sup>-1</sup> to ~10 m d<sup>-1</sup>. These changes hint at a shift towards a more efficient subglacial drainage system in the  
614 lower trunk and resemble early summer slowdowns due to hydrological changes observed during quiescent  
615 years on Sít' Kusá (Liu and others, 2024) and on other Alaskan surge type glaciers during quiescence  
616 (Abe and Furuya, 2015). During this time, correlations between the modelled surface runoff and the  
617 bay turbidity record are generally around  $r=0.5$ , implying some component of the surface runoff travels  
618 through the glacier quickly and affects the bay turbidity levels. From early July to early August 2021,  
619 there are disruptions in coherence in the upper trunk and lags in the lower trunk remain largely below zero,  
620 suggesting a poorly connected drainage system where tremor is generated largely by spatially distributed  
621 surface runoff. The correlation between modelled surface runoff and bay turbidity largely disappears during  
622 this time, with two oscillations with ~10 day periods in the turbidity record that are of similar amplitude  
623 to earlier variations but appear unforced by surface runoff on the glacier. Meanwhile, there are large  
624 variations in daily GNSS velocities (between 2 m d<sup>-1</sup> and 10 m d<sup>-1</sup>) from July 1<sup>st</sup> to August 11<sup>th</sup>. The  
625 periods of speedup coincide with increases in meltwater supply and in seismic tremor. Broadly, our data  
626 seems to reflect a disrupted and relatively low efficiency system during the final weeks of the surge, with  
627 variability in ice velocities driven by changes in water supply from distributed surface runoff. Meanwhile,  
628 the proxy record for sub-aqueous frontal discharge suggest that considerable volumes of water are gradually  
629 released from sub- or englacial storage.

630 In early August, more sustained high coherence returns between the stations framing the lower trunk,  
631 with lags of approximately five hours. From 1 August to 11 August, ice velocities undergo a decreasing  
632 trend from ~10 m d<sup>-1</sup> to ~3 m d<sup>-1</sup> and the turbidity in front of the terminus is gradually increasing,  
633 without significant increases in surface runoff. A rainstorm from 11 August to 14 August 2021 drives  
634 extreme surface runoff, which coincides with a peak in glaciohydraulic tremor and in ice velocities. The

635 rising limbs in the runoff and tremor signals coincide with a peak in ice velocities of  $\sim 16 \text{ m d}^{-1}$ , which is  
636 directly followed by a slowdown to velocities below  $5 \text{ m d}^{-1}$ . The spike in surface runoff, glaciohydraulic  
637 tremor, and ice velocity fits well with previous suggestions of the surge termination process reported in  
638 Kamb and others (1985) and Kamb (1987), where a switch from a linked cavity system to a channelized  
639 drainage system drives surge termination. However, we do not observe any change in the time-lags between  
640 tremor time-series for either the upper or lower trunk. This is remarkable as the time-lags reliably reflect  
641 changes in the drainage system at other moments in our record and it seems likely that we would observe  
642 some change if there was a sudden and widespread switching between drainage system configurations from  
643 11-14 August. Additionally, we do not observe a sudden spike in turbidity that would reflect a sudden  
644 release of large water volumes. The latter might be explained by more gradual prior water release during  
645 July 2021, which rather echoes behavior observed on Svalbard (Murray and others, 2000). Such a gradual  
646 water release, combined with the slowdown in ice velocities from 1 to 11 August and the five hour time-  
647 lags existing from 1 August on-wards, suggest that any switching in drainage systems leading to surge  
648 termination was more gradual on Sít' Kusá than on Variegated Glacier. We suggest some component of  
649 efficient drainage was established by 1 August in the lower trunk. Subsequently, the rainstorm driven influx  
650 of water overwhelmed this existing efficient drainage and led to widespread high basal water pressure and  
651 low effective pressure, driving the peak in ice velocities. The 12-13 August speedup is superimposed on  
652 a trend of gradual slowdown and seems modulated by temporary overloading of the efficient component  
653 of the subglacial drainage system. Such a mechanism is common and well explained on non-surge type  
654 glaciers (e.g. Iken and Bindschadler, 1986; Anderson and others, 2004; Bartholomaus and others, 2008;  
655 Schoof, 2010; Labedz and others, 2022; Hart and others, 2022).

656 During the remainder of the melt season, ice velocities are generally lower and less variable (Fig.8c).  
657 Peaks in surface runoff result in sharp increases in glaciohydraulic tremor with muted responses in ice  
658 velocity variations (Fig.8). Such behavior closely resembles that observed during the late-melt season on  
659 non-surgings alpine glaciers (Nanni and others, 2020; Labedz and others, 2022). Time lags for the lower  
660 trunk remain around five hours until 26 August, then decrease to become slightly negative by 31 August  
661 (Fig.8b). Finally, the surface runoff and bay turbidity signals are highly coherent and vary in phase, as  
662 shown by the consistently high correlation between the two time-series (Fig.8a). We suggest this points to  
663 a drainage system in the lower trunk through which water circulates quickly and where surface runoff is the  
664 dominant supply. The now “low volume” system that lacks significant input from sub- or englacial water

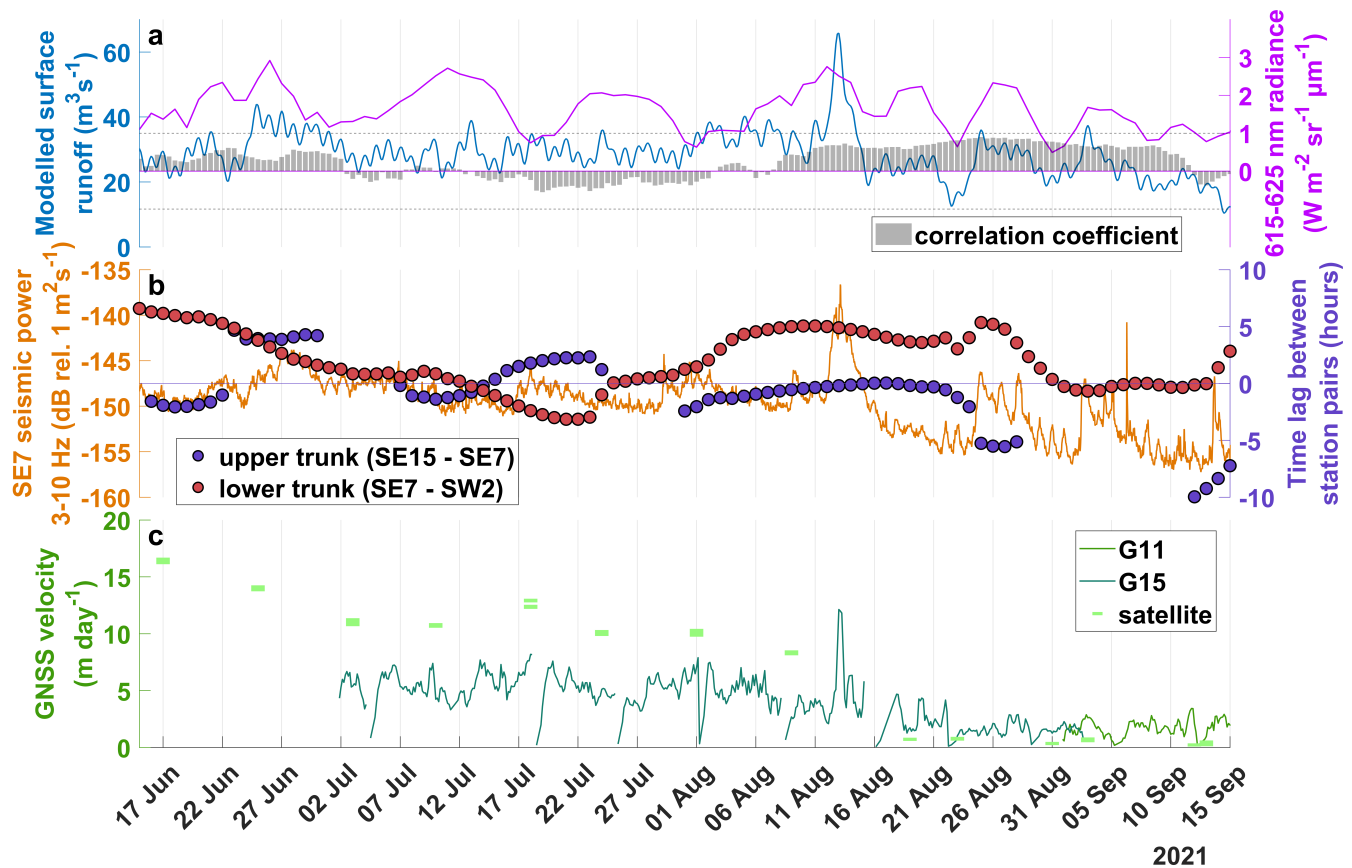


**Fig. 8.** Glacier behavior during the 2021 melt season. a) Modelled surface runoff and average daily water surface radiance measured with Sentinel 3 OLCI. Correlation coefficients calculated between 10 day rolling windows with a 12 hour shift, of both time-series interpolated on a 12 hour interval. b) Median seismic power measured at SE7 and lags between tremor power time-series measured between SE15-SE7 (purple dots) and SE7-SW2 (red dots) station pairs. c) Glacier surface velocity measured with GPS and satellite imagery feature tracking.

665 contributions might be gradually closing under ice overburden pressure by late August 2021, as evidenced  
 666 by the lost coherence in the upper trunk and slightly negative lags in the lower trunk.

667 Our data point to gradual and non-monotonic changes in the drainage system during the 2021 melt  
 668 season that combine towards surge termination. The glacier gradually releases water throughout the  
 669 summer and the 11-14 August rainstorm seems to coincide with the final release and emptying of any sub-  
 670 or englacial reserves. Throughout the summer, changes in surface runoff drive changes in ice velocity on the  
 671 timescale of days, which are superimposed on the trend of surge slowdown. Such variability superimposed  
 672 on longer trends is not exclusive to Sít' Kusá (Benn and others, 2022). This variability shows the drainage  
 673 system is evolving simultaneously at multiple time-scales and conflicts with the notion of a single switch  
 674 marking termination.



675 **SYNTHESIS**

676 Our observations are broadly consistent with existing theoretical mechanisms of glacier surging, but draw  
677 attention to some key points concerning the evolution of the subglacial drainage system during the surge.  
678 On Sít' Kusá there is a component of the subglacial hydrological system that extends along the main  
679 glacier trunk, is connected to the glacier surface, and is intermittently efficient during the active phase. This  
680 component is connected to a large enough area of the glacier base for its evolution to occasionally force high  
681 amplitude variability in ice velocities during the active phase. Similar high variability in surface velocities  
682 is observed during other surges when the temporal resolution of observations is high enough (Beaud and  
683 others, 2022; Benn and others, 2022) and has been linked to variability in basal water pressure (Kamb and  
684 others, 1985). Our data show that this variability can occur as suggested by Kamb and others (1985) during  
685 periods of disrupted, inefficient drainage (e.g. July 2021) but also through the overwhelming of existing  
686 efficient, channelized drainage (e.g. October 2020, August 2021). The second overwhelming mechanism  
687 has been observed repeatedly on non-surging glaciers (e.g. Anderson and others, 2004; Bartholomew and  
688 others, 2012; Cowton and others, 2013) and its presence during an active surge shows there are consistent  
689 mechanisms driving flow velocities throughout the surge cycle.

690 On the timescales of surge evolution, we observe variability in the efficiency of the subglacial system  
691 and possibly short term changes in its configuration but no change in how it fundamentally behaves or  
692 clear evidence of a single widespread switching between configurations. Surge termination during the 2021  
693 summer is a gradual process rather than a sudden switch in behavior. This echoes conclusions drawn for the  
694 slow surging Trapridge Glacier by Frappé and Clarke (2007), where authors hint at an out of equilibrium  
695 but fundamentally unchanged drainage system where subsequent changes in efficiency accumulate into the  
696 observed surge behavior. Benn and others (2022) suggest surge type glaciers might be characterised by a  
697 basal water surplus that is too high to be accommodated by a “slow” system and too low to transition  
698 to a “fast” system. Reciprocally, such a situation would likely lead to the semi-efficient, or intermittently  
699 efficient, drainage system we seem to observe.

700 Finally, we note that there seems to be a shift in the availability of sub- or en-glacially stored water that  
701 occurs with surge termination. We suggest the surge-time drainage system differentiates itself primarily  
702 by an overabundance of available water that is independent of surface runoff, as shown by the continued  
703 water flow during the 2020-2021 winter that contrasts with the 2021-2022 winter. This notion is in line

704 with the observation that overwinter storage of surface runoff allows springtime speedups on Sít' Kusá (Liu  
705 and others, 2024), as well as with earlier work pointing to a potential role for gradual water accumulation  
706 in driving glacier surging (Humphrey and Raymond, 1994; Lingle and Fatland, 2003; Abe and Furuya,  
707 2015). Furthermore, our observations align with the notion that a basal enthalpy surplus, which translates  
708 to a basal water surplus on temperate glaciers, accumulates during quiescence and surge onset. This basal  
709 water surplus then gradually dissipates during the later stages of the surge (Benn and others, 2019a, 2022).

## 710 CONCLUSION

711 Although observing the subglacial environment remains a challenging task, the time-series presented in  
712 this study provide a window into the evolution of subglacial drainage over time, without direct access to  
713 the glacier bed. In particular, we note the novel application of wavelet coherence analysis to leverage phase  
714 lags in median seismic power towards observing subglacial water and pressure pulse migration. While there  
715 are limitations outlined in this study, the approach allows for continuous and remotely sensed monitoring  
716 of changes in the critical (seismically loud) components of the subglacial drainage system.

717 Our observations show that glacier surges can be resilient to continuous, observable, and intermittently  
718 efficient drainage. The channelized components of subglacial drainage can intermittently restrict subglacial  
719 water flow, modulating surge dynamics. These observations conflict with a theory of “hard switching”  
720 between fully efficient and inefficient drainage systems (Kamb, 1987). Nevertheless, they strengthen the  
721 broader applicability of the hydrologically regulated surge mechanism as they provide avenues through  
722 which a drainage system that continues to undergo seasonal and sub-seasonal changes can drive multi-year  
723 surge dynamics (Benn and others, 2022).

724 The evolution of the subglacial drainage system during the observed part of the surge cycle seems to  
725 express itself on a spectrum of efficiency. It underlines complexity and variability on sub-seasonal, seasonal,  
726 and multi-year timescales that interfere to produce the spectacular glacier dynamics on Sít' Kusá. We did  
727 not observe hydrological features that set Sít' Kusá apart from glaciers with steady state flow behavior.  
728 It seems worthwhile to consider whether similar multi-annual velocity variations might be present at all  
729 glaciers, just with lower amplitudes. Such a perspective seems consistent with the emerging notion that  
730 many glaciers not identified strictly as “surging” have complex multi-year velocity patterns (Herreid and  
731 Truffer, 2016). This perhaps suggests that glacier surges are simply the most spectacular, and easiest to  
732 detect, expressions of hydrologically driven periodic velocity variations common to many glaciers.

## 733 DATA AVAILABILITY

734 Code for seismic data processing is available at [doi.org/10.5281/zenodo.8102681](https://doi.org/10.5281/zenodo.8102681). Code for computing time-  
735 lags in glaciohydraulic tremor is repositored at [github.com/yoramterleth/tremor\\_lags](https://github.com/yoramterleth/tremor_lags). Seismic data are  
736 archived at the Earthscope/IRIS DMC (network code: YG) and will be freely available starting January  
737 2026. GNSS data are in the process of being archived through the Earthscope/UNAVCO data reposi-  
738 tory. Time-series of glaciohydraulic tremor, modelled surface runoff and tremor time-lags are available at  
739 DOI:10.5281/zenodo.10525141. Pipelines for accessing and processing ocean surface turbidity in Disen-  
740 chantment Bay are available at: [github.com/yoramterleth/d\\_bay\\_monitoring](https://github.com/yoramterleth/d_bay_monitoring).

## 741 SUPPLEMENTARY MATERIAL

742 The supplementary material for this article can be found at [\[insert link\]](#).

## 743 ACKNOWLEDGEMENTS

744 This project was funded by NSF Award ANS1954021. We thank Kate Bollen, Thomas Otheim, Chris  
745 Miele, Dakota Pyles, Jason Amundson, Jake Anderson, Galen Dossin, Susan Detweiler, and Hans Munich  
746 and Tanya Hutchins at Coastal Airline Services LLC for their roles in the data collection effort. Some  
747 seismic and GNSS instruments were provided by EarthScope Consortium. The facilities of EarthScope  
748 Consortium are supported by the National Science Foundation's Seismological Facility for the Advancement  
749 of Geoscience (SAGE) Award under Cooperative Support Agreement EAR-1851048 and Geodetic Facility  
750 for the Advancement of Geoscience (GAGE) Award under NSF Cooperative Agreement EAR-1724794. We  
751 used Google Earth Engine to analyze satellite imagery acquired through the European Space Agency's  
752 Sentinel Missions. Finally we thank reviewers Doug Benn and Ugo Nanni as well as editors Matthew  
753 Siegfried and Hester Jiskoot for their feedback on this work, which greatly helped improve it.

## 754 REFERENCES

- 755 Abe T and Furuya M (2015) Winter speed-up of quiescent surge-type glaciers in Yukon, Canada. *The Cryosphere*,  
756 **9**(3), 1183–1190 (doi: 10.5194/tc-9-1183-2015)
- 757 Alexander A, Obu J, Schuler TV, Kääh A and Christiansen HH (2020) Subglacial permafrost dynamics and erosion  
758 inside subglacial channels driven by surface events in Svalbard. *The Cryosphere*, **14**(11), 4217–4231

- 759 Anderson RS, Anderson SP, MacGregor KR, Waddington ED, O'Neel S, Riihimaki CA and Loso MG (2004) Strong  
760 feedbacks between hydrology and sliding of a small alpine glacier. *Journal of Geophysical Research: Earth Surface*,  
761 **109**(F3) (doi: 10.1029/2004JF000120)
- 762 Andrews LC, Catania GA, Hoffman MJ, Gulley JD, Lüthi MP, Ryser C, Hawley RL and Neumann TA (2014) Direct  
763 observations of evolving subglacial drainage beneath the Greenland Ice Sheet. *Nature*, **514**(7520), 80–83 (doi:  
764 10.1038/nature13796)
- 765 Bakker M, Gimbert F, Geay T, Misset C, Zanker S and Recking A (2020) Field application and validation of a  
766 seismic bedload transport model. *Journal of Geophysical Research: Earth Surface*, **125**(5), e2019JF005416 (doi:  
767 10.1029/2019JF005416)
- 768 Barrett AP and Collins DN (1997) Interaction between water pressure in the basal drainage system and discharge  
769 from an alpine glacier before and during a rainfall-induced subglacial hydrological event. *Annals of Glaciology*, **24**,  
770 288–292 (doi: 10.3189/S0260305500012325)
- 771 Barrett BE, Murray T, Clark R and Matsuoka K (2008) Distribution and character of water in a surge-type glacier  
772 revealed by multifrequency and multipolarization ground-penetrating radar. *Journal of Geophysical Research:*  
773 *Earth Surface*, **113**(F4) (doi: 10.1029/2007JF000972)
- 774 Bartholomaus TC and Terleth Y (2023) med\_spec: Calculation of median seismic spectrograms, for purposes of  
775 quantifying tremor (doi: 10.5281/zenodo.8102681)
- 776 Bartholomaus TC, Anderson RS and Anderson SP (2008) Response of glacier basal motion to transient water storage.  
777 *Nature Geoscience*, **1**(1), 33–37 (doi: 10.1038/ngeo.2007.52)
- 778 Bartholomaus TC, Larsen CF, O'Neel S and West ME (2012) Calving seismicity from iceberg–sea surface interactions.  
779 *Journal of Geophysical Research: Earth Surface*, **117**(F4) (doi: 10.1029/2012JF002513)
- 780 Bartholomaus TC, Larsen CF and O'Neel S (2013) Does calving matter? Evidence for significant submarine melt.  
781 *Earth and Planetary Science Letters*, **380**, 21–30 (doi: 10.1016/j.epsl.2013.08.014)
- 782 Bartholomaus TC, Amundson JM, Walter JJ, O'Neel S, West ME and Larsen CF (2015) Subglacial discharge at  
783 tidewater glaciers revealed by seismic tremor. *Geophysical Research Letters*, **42**(15), 6391–6398 (doi: 10.1002/  
784 2015GL064590)
- 785 Bartholomew I, Nienow P, Sole A, Mair D, Cowton T and King MA (2012) Short-term variability in Greenland  
786 Ice Sheet motion forced by time-varying meltwater drainage: Implications for the relationship between subglacial  
787 drainage system behavior and ice velocity. *Journal of Geophysical Research: Earth Surface*, **117**(F3) (doi: 10.  
788 1029/2011JF002220)

- 789 Beaud F, Flowers GE and Venditti JG (2018) Modeling sediment transport in ice-walled subglacial channels and its  
790 implications for esker formation and proglacial sediment yields. *Journal of Geophysical Research: Earth Surface*,  
791 **123**(12), 3206–3227 (doi: 10.1029/2018JF004779)
- 792 Beaud F, Aati S, Delaney I, Adhikari S and Avouac JP (2022) Surge dynamics of Shisper Glacier revealed by  
793 time-series correlation of optical satellite images and their utility to substantiate a generalized sliding law. *The*  
794 *Cryosphere*, **16**(8), 3123–3148 (doi: 10.5194/tc-16-3123-2022)
- 795 Benn D, Fowler AC, Hewitt I and Sevestre H (2019a) A general theory of glacier surges. *Journal of Glaciology*,  
796 **65**(253), 701–716 (doi: 10.1017/jog.2019.62)
- 797 Benn DI, Jones RL, Luckman A, Fürst JJ, Hewitt I and Sommer C (2019b) Mass and enthalpy budget evolution  
798 during the surge of a polythermal glacier: a test of theory. *Journal of Glaciology*, **65**(253), 717–731 (doi: 10.1017/  
799 jog.2019.63)
- 800 Benn DI, Hewitt IJ and Luckman AJ (2022) Enthalpy balance theory unifies diverse glacier surge behaviour. *Annals*  
801 *of Glaciology*, **63**(87-89), 88–94 (doi: 10.1017/aog.2023.23)
- 802 Chu VW, Smith LC, Rennermalm AK, Forster RR, Box JE and Reeh N (2009) Sediment plume response to surface  
803 melting and supraglacial lake drainages on the Greenland ice sheet. *Journal of Glaciology*, **55**(194), 1072–1082  
804 (doi: 10.3189/002214309790794904)
- 805 Church G, Bauder A, Grab M and Maurer H (2021) Ground-penetrating radar imaging reveals glacier’s drainage  
806 network in 3d. *The Cryosphere*, **15**(8), 3975–3988 (doi: 10.5194/tc-15-3975-2021)
- 807 Clarke GK, Collins SG and Thompson DE (1984) Flow, thermal structure, and subglacial conditions of a surge-type  
808 glacier. *Canadian Journal of Earth Sciences*, **21**(2), 232–240 (doi: 10.1139/e84-024)
- 809 Clarke GKC (1996) Lumped-element analysis of subglacial hydraulic circuits. *Journal of Geophysical Research: Solid*  
810 *Earth*, **101**(B8), 17547–17559 (doi: 10.1029/96JB01508)
- 811 Cowton T, Nienow P, Sole A, Wadham J, Lis G, Bartholomew I, Mair D and Chandler D (2013) Evolution of  
812 drainage system morphology at a land-terminating Greenlandic outlet glacier. *Journal of Geophysical Research:*  
813 *Earth Surface*, **118**(1), 29–41 (doi: 10.1029/2012JF002540)
- 814 Dunse T, Schellenberger T, Hagen JOM, Käab A, Schuler TV and Reijmer C (2015) Glacier-surge mecha-  
815 nisms promoted by a hydro-thermodynamic feedback to summer melt. *The Cryosphere*, **9**, 197–215 (doi:  
816 10.5194/tc-9-197-2015)
- 817 ESA (2022a) Sentinel-1 SAR technical guide. ([https://sentinels.copernicus.eu/web/sentinel/technical-](https://sentinels.copernicus.eu/web/sentinel/technical-guides/sentinel-1-sar)  
818 [guides/sentinel-1-sar](https://sentinels.copernicus.eu/web/sentinel/technical-guides/sentinel-1-sar), last accessed on 11/04/2024)

- 819 ESA (2022b) Sentinel-2 MSI technical guide. ([https://sentinels.copernicus.eu/web/sentinel/technical-guides/sentinel-](https://sentinels.copernicus.eu/web/sentinel/technical-guides/sentinel-2-msi)  
820 2-msi, last accessed on 11/04/2024)
- 821 ESA (2022c) Sentinel-3 OLCI technical guide. ([https://sentinels.copernicus.eu/web/sentinel/technical-](https://sentinels.copernicus.eu/web/sentinel/technical-guides/sentinel-3-olci)  
822 guides/sentinel-3-olci, last accessed on 11/04/2024)
- 823 Ferdous MS, McGuire P, Power D, Johnson T and Collins M (2018) A comparison of numerically modelled iceberg  
824 backscatter signatures with Sentinel-1 C-Band Synthetic Aperture Radar acquisitions. *Canadian Journal of Remote*  
825 *Sensing*, **44**(3), 232–242 (doi: 10.1080/07038992.2018.1495554)
- 826 Flowers GE and Clarke GKC (2002) A multicomponent coupled model of glacier hydrology 2. Application to Trapridge  
827 Glacier, Yukon, Canada. *Journal of Geophysical Research: Solid Earth*, **107**(B11), ECV 10–1–ECV 10–16 (doi:  
828 10.1029/2001JB001124)
- 829 Frappé TP and Clarke GK (2007) Slow surge of Trapridge Glacier, Yukon Territory, Canada. *Journal of Geophysical*  
830 *Research: Earth Surface*, **112**(F3) (doi: 10.1029/2006JF000607)
- 831 Fried MJ, Catania GA, Stearns LA, Sutherland DA, Bartholomaeus TC, Shroyer E and Nash J (2018) Reconciling  
832 drivers of seasonal terminus advance and retreat at 13 Central West Greenland tidewater glaciers. *Journal of*  
833 *Geophysical Research: Earth Surface*, **123**(7), 1590–1607 (doi: 10.1029/2018JF004628)
- 834 Gimbert F, Tsai VC and Lamb MP (2014) A physical model for seismic noise generation by turbulent flow in rivers.  
835 *Journal of Geophysical Research: Earth Surface*, **119**(10), 2209–2238 (doi: 10.1002/2014JF003201)
- 836 Gimbert F, Tsai VC, Amundson JM, Bartholomaeus TC and Walter JI (2016) Subseasonal changes observed in  
837 subglacial channel pressure, size, and sediment transport. *Geophysical Research Letters*, **43**(8), 3786–3794 (doi:  
838 10.1002/2016GL068337)
- 839 Gimbert F, Nanni U, Roux P, Helmstetter A, Garambois S, Lecointre A, Walpersdorf A, Jourdain B, Langlais M,  
840 Laarman O and others (2021) A multi-physics experiment with a temporary dense seismic array on the Argentière  
841 glacier, French Alps: The RESOLVE project. *Seismological Research Letters*, **92**(2A), 1185–1201 (doi: 10.1785/  
842 0220200280)
- 843 Goff JA, Lawson DE, Willems BA, Davis M and Gulick SPS (2012) Morainal bank progradation and sediment  
844 accumulation in Disenchantment Bay, Alaska: Response to advancing Hubbard Glacier. *Journal of Geophysical*  
845 *Research: Earth Surface*, **117**(F2) (doi: 10.1029/2011JF002312)
- 846 Gong Y, Zwinger T, Åström J, Altena B, Schellenberger T, Gladstone R and Moore J (2018) Simulating the roles  
847 of crevasse routing of surface water and basal friction on the surge evolution of Basin 3, Austfonna ice cap. *The*  
848 *Cryosphere* (doi: 10.5194/tc-12-1563-2018)



- 849 Grinsted A, Moore JC and Jevrejeva S (2004) Application of the cross wavelet transform and wavelet coherence to  
850 geophysical time series. *Nonlinear Processes in Geophysics*, **11**(5/6), 561–566 (doi: 10.5194/npg-11-561-2004)
- 851 Gulley JD, Walthard P, Martin J, Banwell AF, Benn DI and Catania G (2012) Conduit roughness and dye-trace  
852 breakthrough curves: why slow velocity and high dispersivity may not reflect flow in distributed systems. *Journal*  
853 *of Glaciology*, **58**(211), 915–925 (doi: 10.3189/2012JoG11J115)
- 854 Hamilton GS and Dowdeswell JA (1996) Controls on glacier surging in Svalbard. *Journal of Glaciology*, **42**(140),  
855 157–168 (doi: 10.3189/S0022143000030616)
- 856 Harrison W and Post A (2003) How much do we really know about glacier surging? *Annals of glaciology*, **36**, 1–6  
857 (doi: 10.3189/172756403781816185)
- 858 Hart JK, Young DS, Baurley NR, Robson BA and Martinez K (2022) The seasonal evolution of subglacial  
859 drainage pathways beneath a soft-bedded glacier. *Communications Earth & Environment*, **3**(1), 1–13 (doi:  
860 10.1038/s43247-022-00484-9)
- 861 Herreid S and Truffer M (2016) Automated detection of unstable glacier flow and a spectrum of speedup behavior in  
862 the Alaska Range. *Journal of Geophysical Research: Earth Surface*, **121**(1), 64–81 (doi: 10.1002/2015JF003502)
- 863 Hock R and Hooke RL (1993) Evolution of the internal drainage system in the lower part of the ablation area  
864 of Storglaciären, Sweden. *GSA Bulletin*, **105**(4), 537–546 (doi: 10.1130/0016-7606(1993)105<0537:EOTIDS>2.3.  
865 CO;2)
- 866 Hossain A, Mathias C and Blanton R (2021) Remote sensing of turbidity in the Tennessee river using Landsat 8  
867 satellite. *Remote Sensing*, **2021**, 3785 (doi: 10.3390/rs13183785)
- 868 Humphrey NF and Raymond C (1994) Hydrology, erosion and sediment production in a surging glacier: Variegated  
869 Glacier, Alaska, 1982–83. *Journal of Glaciology*, **40**(136), 539–552 (doi: 10.3189/S0022143000012429)
- 870 Iken A (1981) The effect of the subglacial water pressure on the sliding velocity of a glacier in an idealized numerical  
871 model. *Journal of Glaciology*, **27**(97), 407–421 (doi: 10.3189/S0022143000011448)
- 872 Iken A and Bindschadler RA (1986) Combined measurements of subglacial water pressure and surface velocity of  
873 Findelengletscher, Switzerland: conclusions about drainage system and sliding mechanism. *Journal of Glaciology*,  
874 **32**(110), 101–119 (doi: 10.3189/S0022143000006936)
- 875 Iken A and Truffer M (1997) The relationship between subglacial water pressure and velocity of Findelen-  
876 gletscher, Switzerland, during its advance and retreat. *Journal of Glaciology*, **43**(144), 328–338 (doi: 10.3189/  
877 S0022143000003282)

- 878 Iverson NR (2010) Shear resistance and continuity of subglacial till: hydrology rules. *Journal of Glaciology*, **56**(200),  
879 1104–1114 (doi: 10.3189/002214311796406220)
- 880 Kamb B (1987) Glacier surge mechanism based on linked cavity configuration of the basal water conduit system.  
881 *Journal of Geophysical Research: Solid Earth*, **92**(B9), 9083–9100 (doi: 10.1029/JB092iB09p09083)
- 882 Kamb B, Raymond C, Harrison W, Engelhardt H, Echelmeyer K, Humphrey N, Brugman M and Pfeffer T (1985)  
883 Glacier surge mechanism: 1982–1983 surge of Variegated Glacier, Alaska. *Science*, **227**(4686), 469–479 (doi: 10.  
884 1126/science.227.4686.469)
- 885 Kotlyakov VM, Rototaeva O and Nosenko G (2004) The September 2002 Kolka glacier catastrophe in North Ossetia,  
886 Russian Federation: evidence and analysis. *Mountain Research and Development*, **24**(1), 78–83 (doi: 10.1659/  
887 0276-4741(2004)024[0078:TSKGCI]2.0.CO;2)
- 888 Kyrke-Smith TM, Katz RF and Fowler AC (2014) Subglacial hydrology and the formation of ice streams. *Proceedings*  
889 *of the Royal Society A: Mathematical, Physical and Engineering Sciences*, **470**(2161), 20130494 (doi: 10.1098/rspa.  
890 2013.0494)
- 891 Köpfli M, Gräff D, Lipovsky BP, Selvadurai PA, Farinotti D and Walter F (2022) Hydraulic conditions for stick-  
892 slip tremor beneath an alpine glacier. *Geophysical Research Letters*, **49**(21), e2022GL100286 (doi: 10.1029/  
893 2022GL100286)
- 894 Labedz CR, Bartholomaeus TC, Amundson JM, Gimbert F, Karplus MS, Tsai VC and Veitch SA (2022) Seismic map-  
895 ping of subglacial hydrology reveals previously undetected pressurization event. *Journal of Geophysical Research:*  
896 *Earth Surface*, **127**(3), e2021JF006406 (doi: 10.1029/2021JF00640)
- 897 Lei Y, Gardner A and Agram P (2021) Autonomous Repeat Image Feature Tracking (autoRIFT) and its application  
898 for tracking ice displacement. *Remote Sensing*, **13**(4), 749 (doi: 10.3390/rs13040749)
- 899 Lindner F, Walter F, Laske G and Gimbert F (2020) Glaciohydraulic seismic tremors on an Alpine glacier. *The*  
900 *Cryosphere*, **14**(1), 287–308 (doi: 10.5194/tc-14-287-2020)
- 901 Lingle CS and Fatland DR (2003) Does englacial water storage drive temperate glacier surges? *Annals of Glaciology*,  
902 **36**, 14–20 (doi: 10.3189/172756403781816464)
- 903 Lipovsky BP and Dunham EM (2017) Slow-slip events on the Whillans Ice Plain, Antarctica, described using rate-  
904 and-state friction as an ice stream sliding law. *Journal of Geophysical Research: Earth Surface*, **122**(4), 973–1003  
905 (doi: 10.1002/2016JF004183)

- 906 Liu J, Enderlin EM, Bartholomaus TC, Terleth Y, Mikesell TD and Beaud F (2024) Propagating speedups during  
907 quiescence escalate to the 2020–2021 surge of Sít’Kusá, southeast Alaska. *Journal of Glaciology*, 1–12 (doi: 10.  
908 1017/jog.2023.99)
- 909 Lliboutry L (1968) General theory of subglacial cavitation and sliding of temperate glaciers. *Journal of Glaciology*,  
910 **7**(49), 21–58 (doi: 10.3189/S0022143000020396)
- 911 McGrath D, Steffen K, Overeem I, Mernild SH, Hasholt B and Broeke MVD (2010) Sediment plumes as a proxy  
912 for local ice-sheet runoff in Kangerlussuaq Fjord, West Greenland. *Journal of Glaciology*, **56**(199), 813–821 (doi:  
913 10.3189/002214310794457227)
- 914 McNamara DE and Buland RP (2004) Ambient noise levels in the continental United States. *Bulletin of the Seis-*  
915 *mological Society of America*, **94**(4), 1517–1527 (doi: 10.1785/012003001)
- 916 Meier MF and Post A (1969) What are glacier surges? *Canadian Journal of Earth Sciences*, **6**(4), 807–817 (doi:  
917 10.1139/e69-081)
- 918 Millan R, Mouginit J, Rabatel A and Morlighem M (2022) Ice velocity and thickness of the world’s glaciers. *Nature*  
919 *Geoscience*, **15**, 124–129 (doi: 10.1038/s41561-021-00885-z)
- 920 Minchew B and Meyer CR (2020) Dilation of subglacial sediment governs incipient surge motion in glaciers with  
921 deformable beds. *Proceedings of the Royal Society A*, **476**(2238), 2020–0033 (doi: 10.1098/rspa.2020.0033)
- 922 Moon T, Joughin I, Smith B, van den Broeke MR, van de Berg WJ, Noël B and Usher M (2014) Distinct patterns of  
923 seasonal Greenland glacier velocity. *Geophysical Research Letters*, **41**(20), 7209–7216 (doi: 10.1002/2014GL061836)
- 924 Murray T, Stuart GW, Miller PJ, Woodward J, Smith AM, Porter PR and Jiskoot H (2000) Glacier surge propagation  
925 by thermal evolution at the bed. *Journal of Geophysical Research: Solid Earth*, **105**(B6), 13491–13507 (doi:  
926 10.1029/2000JB900066)
- 927 Nanni U, Gimbert F, Vincent C, Gräff D, Walter F, Piard L and Moreau L (2020) Quantification of seasonal and  
928 diurnal dynamics of subglacial channels using seismic observations on an Alpine glacier. *The Cryosphere*, **14**(5),  
929 1475–1496 (doi: 10.5194/tc-14-1475-2020)
- 930 Nanni U, Gimbert F, Roux P and Lecointre A (2021) Observing the subglacial hydrology network and its dynamics  
931 with a dense seismic array. *Proceedings of the National Academy of Sciences*, **118**(28), e2023757118 (doi: 10.1073/  
932 pnas.2023757118)
- 933 Nanni U, Roux P, Gimbert F and Lecointre A (2022) Dynamic imaging of glacier structures at high-resolution  
934 using source localization with a dense seismic array. *Geophysical Research Letters*, **49**(6), e2021GL095996 (doi:  
935 10.1029/2021GL095996)

- 936 Nolan A, Kochtitzky W, Enderlin EM, McNabb R and Kreutz KJ (2021) Kinematics of the exceptionally-short surge  
937 cycles of Sit Kusa (Turner Glacier), Alaska, from 1983 to 2013. *Journal of Glaciology*, **67**(264), 744–758 (doi:  
938 10.1017/jog.2021.29)
- 939 Nye JF (1976) Water Flow in Glaciers: Jökulhlaups, Tunnels and Veins. *Journal of Glaciology*, **17**(76), 181–207 (doi:  
940 10.3189/S002214300001354X)
- 941 O’Neel S and Pfeffer W (2007) Source mechanics for monochromatic icequakes produced during iceberg calving at  
942 Columbia Glacier, AK. *Geophysical Research Letters*, **34**(22)
- 943 Podolskiy EA, Murai Y, Kanna N and Sugiyama S (2021) Ocean-bottom and surface seismometers reveal continuous  
944 glacial tremor and slip. *Nature Communications*, **12**(1), 3929 (doi: 10.1038/s41467-021-24142-4)
- 945 Porter C, Morin P, Howat I, Noh MJ, Bates B, Peterman K, Keesey S, Schlenk M, Gardiner J, Tomko K and others  
946 (2018) ArcticDEM. *Harvard Dataverse*, **1**, 2018–30 (doi: 10.7910/DVN/OHHUKH)
- 947 Rada C and Schoof C (2018) Channelized, distributed, and disconnected: subglacial drainage under a valley glacier  
948 in the Yukon. *The Cryosphere*, **12**(8), 2609–2636 (doi: 10.5194/tc-12-2609-2018)
- 949 Röthlisberger H (1972) Water pressure in intra- and subglacial channels. *Journal of Glaciology*, **11**(62), 177–203 (doi:  
950 10.3189/S0022143000022188)
- 951 Schild KM, Hawley RL, Chipman JW and Benn DI (2017) Quantifying suspended sediment concentration in sub-  
952 glacial sediment plumes discharging from two svalbard tidewater glaciers using landsat-8 and in situ measurements.  
953 *International Journal of Remote Sensing*, **38**(23), 6865–6881 (doi: 10.1080/01431161.2017.1365388)
- 954 Schoof C (2010) Ice-sheet acceleration driven by melt supply variability. *Nature*, **468**(7325), 803–806 (doi: 10.1038/  
955 nature09618)
- 956 Schwanghart W and Scherler D (2014) Short Communication: TopoToolbox 2 – MATLAB-based software for to-  
957 pographic analysis and modeling in Earth surface sciences. *Earth Surface Dynamics*, **2**(1), 1–7 (doi: 10.5194/  
958 esurf-2-1-2014)
- 959 Sevestre H and Benn DI (2015) Climatic and geometric controls on the global distribution of surge-type glaciers: im-  
960 plications for a unifying model of surging. *Journal of Glaciology*, **61**(228), 646–662 (doi: 10.3189/2015JoG14J136)
- 961 Sevestre H, Benn DI, Luckman A, Nuth C, Kohler J, Lindbäck K and Pettersson R (2018) Tidewater glacier surges  
962 initiated at the terminus. *Journal of Geophysical Research: Earth Surface*, **123**(5), 1035–1051 (doi: 10.1029/  
963 2017JF004358)

- 964 Shelly DR, Beroza GC, Ide S and Nakamura S (2006) Low-frequency earthquakes in Shikoku, Japan, and their  
965 relationship to episodic tremor and slip. *Nature*, **442**(7099), 188–191 (doi: 10.1038/nature04931)
- 966 Shreve RL (1972) Movement of water in glaciers. *Journal of Glaciology*, **11**(62), 205–214 (doi: 10.3189/  
967 S002214300002219X)
- 968 Sikonia WG and Post A (1980) Columbia Glacier, Alaska: Recent ice loss and its relationship to seasonal terminal  
969 embayments, thinning, and glacial flow. USGS Numbered Series 619, U.S. Geological Survey
- 970 Simpson JJ, Hufford GL, Daly C, Berg JS and Fleming MD (2005) Comparing maps of mean monthly surface  
971 temperature and precipitation for Alaska and adjacent areas of Canada produced by two different methods. *Arctic*,  
972 **58**(2), 137–161
- 973 Sundal AV, Shepherd A, Nienow P, Hanna E, Palmer S and Huybrechts P (2011) Melt-induced speed-up of Greenland  
974 ice sheet offset by efficient subglacial drainage. *Nature*, **469**(7331), 521–524 (doi: 10.1038/nature09740)
- 975 Tape C, Heath DC, Baker MG, Dalton S, Aderhold K and West ME (2019) Bear encounters with seismic stations in  
976 Alaska and northwestern Canada. *Seismological Research Letters*, **90**(5), 1950–1970 (doi: 10.1785/0220190081)
- 977 Tedstone AJ and Arnold NS (2012) Automated remote sensing of sediment plumes for identification of runoff from  
978 the Greenland ice sheet. *Journal of Glaciology*, **58**(210), 699–712 (doi: 10.3189/2012JoG11J204)
- 979 Terleth Y, Van Pelt W, Pohjola V and Pettersson R (2021) Complementary approaches towards a universal model  
980 of glacier surges. *Frontiers in Earth Science*, **9** (doi: 10.3389/feart.2021.732962)
- 981 Thøgersen K, Gilbert A, Schuler TV and Malthe-Sørenssen A (2019) Rate-and-state friction explains glacier surge  
982 propagation. *Nature communications*, **10**(1), 1–8 (doi: 10.1038/s41467-019-10506-4)
- 983 Truffer M, Harrison WD and Echelmeyer KA (2000) Glacier motion dominated by processes deep in underlying till.  
984 *Journal of Glaciology*, **46**(153), 213–221 (doi: 10.3189/172756500781832909)
- 985 Truffer M, Kääh A, Harrison WD, Osipova GB, Nosenko GA, Espizua L, Gilbert A, Fischer L, Huggel C, Craw Burns  
986 PA and Lai AW (2021) Chapter 13 - Glacier surges. In W Haeberli and C Whiteman (eds.), *Snow and Ice-  
987 Related Hazards, Risks, and Disasters (Second Edition)*, Hazards and Disasters Series, 417–466, Elsevier (doi:  
988 10.1016/B978-0-12-817129-5.00003-2)
- 989 Tsai VC, Minchew B, Lamb MP and Ampuero JP (2012) A physical model for seismic noise generation from sediment  
990 transport in rivers. *Geophysical Research Letters*, **39**(2) (doi: 10.1029/2011GL050255)
- 991 Tulaczyk S, Kamb WB and Engelhardt HF (2000) Basal mechanics of Ice Stream B, west Antarctica: 2. Undrained  
992 plastic bed model. *Journal of Geophysical Research: Solid Earth*, **105**(B1), 483–494 (doi: 10.1029/1999JB900328)

- 993 Vallot D, Pettersson R, Luckman A, Benn DI, Zwinger T, Pelt WJJV, Kohler J, Schäfer M, Claremar B and Hulton  
994 NRJ (2017) Basal dynamics of Kronebreen, a fast-flowing tidewater glacier in Svalbard: non-local spatio-temporal  
995 response to water input. *Journal of Glaciology*, **63**(242), 1012–1024 (doi: 10.1017/jog.2017.69)
- 996 van Pelt W, Oerlemans J, Reijmer C, Pohjola V, Pettersson R and Van Angelen J (2012) Simulating melt, runoff  
997 and refreezing on Nordenskiöldbreen, Svalbard, using a coupled snow and energy balance model. *The Cryosphere*,  
998 **6**(3), 641–659 (doi: 10.5194/tc-6-641-2012)
- 999 van Pelt WJ and Oerlemans J (2012) Numerical simulations of cyclic behaviour in the Parallel Ice Sheet Model  
1000 (PISM). *Journal of Glaciology*, **58**(208), 347–360 (doi: 10.3189/2012JoG11J217)
- 1001 van Pelt WJ, Pohjola VA and Reijmer CH (2016) The changing impact of snow conditions and refreezing on the  
1002 mass balance of an idealized svalbard glacier. *Frontiers in Earth Science*, **4**, 102 (doi: 10.3389/feart.2016.00102)
- 1003 van Pelt WJ, Pohjola VA, Pettersson R, Ehwald LE, Reijmer CH, Boot W and Jakobs CL (2018) Dynamic response  
1004 of a high arctic glacier to melt and runoff variations. *Geophysical Research Letters*, **45**(10), 4917–4926 (doi: 10.  
1005 1029/2018GL077252)
- 1006 van Pelt WJ, Schuler TV, Pohjola VA and Pettersson R (2021) Accelerating future mass loss of Svalbard glaciers  
1007 from a multi-model ensemble. *Journal of Glaciology*, 1–15 (doi: 10.1017/jog.2021.2)
- 1008 Vore ME, Bartholomaus TC, Winberry JP, Walter JI and Amundson JM (2019) Seismic tremor reveals spatial  
1009 organization and temporal changes of subglacial water system. *Journal of Geophysical Research: Earth Surface*,  
1010 **124**(2), 427–446 (doi: 10.1029/2018JF004819)
- 1011 Walder JS (1986) Hydraulics of subglacial cavities. *Journal of Glaciology*, **32**(112), 439–445 (doi: 10.3189/  
1012 S0022143000012156)
- 1013 Walder JS and Fowler A (1994) Channelized subglacial drainage over a deformable bed. *Journal of Glaciology*,  
1014 **40**(134), 3–15 (doi: 10.3189/S0022143000003750)
- 1015 Weertman J (1972) General theory of water flow at the base of a glacier or ice sheet. *Reviews of Geophysics*, **10**(1),  
1016 287–333 (doi: 10.1029/RG010i001p00287)
- 1017 Zhan Z (2019) Seismic noise interferometry reveals transverse drainage configuration beneath the surging Bering  
1018 Glacier. *Geophysical Research Letters*, **46**(9), 4747–4756 (doi: 10.1029/2019GL082411)
- 1019 Zoet LK and Iverson NR (2015) Experimental determination of a double-valued drag relationship for glacier sliding.  
1020 *Journal of Glaciology*, **61**(225), 1–7 (doi: 10.3189/2015JoG14J174)
- 1021 Zoet LK and Iverson NR (2020) A slip law for glaciers on deformable beds. *Science*, **368**(6486), 76–78 (doi: 10.1126/  
1022 science.aaz1183)